

UTRECHT UNIVERSITY

MASTER THESIS

Exploring Cosmic Censorship through Gauge/Gravity Duality

Author:
Marc Aragonès Fontboté

Supervisor:
Dr. Wilke van der Schee

Daily supervisor:
Dr. Javier Subils



**Utrecht
University**

*A thesis submitted in fulfillment of the requirements
for the degree of Master in Theoretical Physics*

in the

Institute of Theoretical Physics
Utrecht University

July 12, 2024

UTRECHT UNIVERSITY

*Abstract*Institute of Theoretical Physics
Utrecht University

Master in Theoretical Physics

Exploring Cosmic Censorship through Gauge/Gravity Duality

by Marc Aragonès Fontboté

We dynamically explore the Cosmic Censorship conjecture by studying asymptotically AdS solutions to Einstein-dilaton gravity in a boost-invariant setup. Our investigation reveals that even though a singularity is only found in the strict $\tau \rightarrow \infty$ limit, curvature invariants grow arbitrarily in an extended region of spacetime, for a generic range of initial conditions. This signals the breakdown of General Relativity, necessitating higher curvature corrections that become relevant within finite time. Hence, making quantum gravity effects significant and observable in a sizable region. Through gauge/gravity duality, we map these dynamics to fluid dynamics on the boundary, where higher curvature terms in the action correspond to finite N and finite coupling corrections, indicating stringy and quantum corrections in the holographic description of the dual plasma.

Acknowledgements

First and foremost, I want to express my deepest gratitude to my supervisor, Wilke van der Schee, for accepting me as a Master student, for allowing me to choose my own project, and for his unwavering guidance and kindness throughout the development of this thesis. I am also grateful for his support in my PhD applications, including all the recommendation letters he wrote for me, which were a lot.

I am deeply thankful to Javi Gómez Subils for accepting the role of being my daily supervisor. His boundless help and patience, along with his encouragement and motivation when the results seemed distant, have been invaluable. The door of his office has always been open to me, and I truly appreciated it.

I extend my sincere thanks to Guillem Pérez Martín for our weekly chats and insightful comments. Your encouragement made this project significantly easier. Thank you for being an invaluable part of this journey, and best of luck in your new adventures.

I am also grateful to David Mateos for guiding the idea, asking the right questions, and suggesting fruitful directions for this project.

I have learned a great deal from each of you. Together, we have formed a nice team, and I am incredibly proud of our collaboration.

I also want to thank all my friends from the Master's program, both Dutch and international, for sharing great experiences and growing together. Especially, I want to thank Pedro Vicente Marto for all the quality time that we shared and all the voluntary donations we made to Casa Ferreira, Kebab Factory, Daily Poké Bowl and O'Panuozzo. To every person that has been part of this amazing 2 year journey, thank you. I had so much fun and I bring every of you in my heart.

Let me now move on to the most important people in my life. Firstly, I want to express my heartfelt gratitude to Nerea, my beloved girlfriend, for always believing in me, even when I doubted myself. Thank you for your unwavering support and love from a distance. It has been challenging, and not everyone believed in us, but we did it. The future is ours now.

Finally, and most importantly, my deepest acknowledgment goes to my parents. None of this would have been possible without you. Thank you for giving me the opportunity to follow my dreams. This thesis is dedicated to you.

Contents

Acknowledgements	v
1 Introduction	1
1.1 Quantum corrections in GR	1
1.2 Cosmic censorship	2
1.2.1 Cosmic censorship violation	3
1.3 Goal of this thesis	4
1.4 Structure of this thesis	5
2 The gauge/gravity duality	7
2.1 Introduction	7
2.2 All you need to know about string theory	7
2.3 Anti-de Sitter spacetime	8
2.4 The large N expansion	9
2.5 Gauge/gravity duality conjecture	9
3 The holographic model	11
3.1 The setup	11
3.1.1 The potential	11
3.1.2 UV physics	12
Note on the conformal dimension Δ of an operator	13
Note on the negative squared mass of the scalar field	13
3.1.3 IR physics	14
3.2 Static Solutions	15
3.2.1 The metric ansatz	15
3.2.2 Near boundary expansion	15
3.2.3 Near horizon expansion	16
3.2.4 Numerical integration	16
3.3 Thermodynamics	18
3.3.1 Holographic renormalization	18
3.3.2 Bekenstein-Hawking entropy	19
3.3.3 Hawking Temperature	20
3.4 Equation of state	21
3.4.1 Low energy limit	22
3.4.2 Equation of state for different γ 's	23
3.5 Transport coefficients	24
3.5.1 Low energy limit	24
4 Hydrodynamics and quark-gluon plasma	27
4.1 Dynamics of relativistic collisions	27
4.1.1 A model for quark-gluon plasma	28
4.2 Hydrodynamics	29
4.3 Ideal Bjorken flow	30

4.4	Ideal non-conformal Bjorken flow	31
4.4.1	Black brane solution	31
4.4.2	Late time thermodynamics	32
4.5	Viscous corrections to non-conformal Bjorken flow	33
4.5.1	Full solution	35
	Late time expansion	35
5	Full microscopic evolution	39
5.1	Dynamic solutions	39
5.1.1	Characteristic formulation of General Relativity	39
5.1.2	The bulk metric ansatz	39
5.1.3	Gauge Freedom	40
5.1.4	Nested structure	40
5.1.5	Near boundary expansion	41
5.1.6	Gauge Fixing	42
5.1.7	Field redefinitions	43
5.1.8	Evolution Algorithm	43
5.1.9	Discretization and spectral methods	44
5.2	Thermodynamics	45
5.2.1	Bekenstein-Hawking entropy	45
5.2.2	Hawking Temperature	46
5.2.3	Holographic renormalization	47
5.3	Code performance	50
5.3.1	Apparent Horizon	50
5.3.2	Convergence	51
5.3.3	Curvatures	51
5.3.4	Energy-Momentum Tensor Conservation	53
6	Cosmic Censorship	57
6.1	Analytical late time behaviour of curvature invariants	58
6.2	Numerical results	60
6.2.1	General vs fined tuned conditions	61
7	Conclusions and future directions	63
7.1	Conclusions	63
7.2	Future directions	63
	Bibliography	65

Als meus pares

Chapter 1

Introduction

Our current understanding of the Universe at the most fundamental level relies on two distinct frameworks. General Relativity (GR), a classical theory, accurately describes gravitational interactions on large, macroscopic scales. In contrast, the other three known fundamental forces—electromagnetic, weak, and strong interactions—are precisely described by a quantum field theory (QFT) known as the Standard Model of elementary particles.

GR is a well-established theory that has passed numerous experimental tests, particularly in scenarios where spacetime curvatures are small. However, the validity of GR in the strong field regime, where direct experiments are lacking, remains uncertain. Moreover, several reasons indicate that GR cannot be the final word in our understanding of gravity. Firstly, because GR predicts its own breakdown, as evidenced by the presence of singularities in the interiors of black holes (BH) or at the Big Bang. Secondly, because it has proven very difficult to make the gravitational interaction compatible with the other three fundamental interactions. All this suggests that a UV completion of GR, namely a quantum theory of gravity, is still lacking.

Remarkably, there is a candidate theory of quantum gravity that not only unifies quantum mechanics with gravity in an elegant and unique framework but also suggests that "gravity is inevitably forced upon us," as Edward Witten famously stated [63]. This theory, known as **string theory**, proposes that the fundamental constituents of the universe are not point-like particles but one-dimensional extended objects called strings. The various quantum modes of vibration of these strings give rise to the different particles observed in nature. Despite its theoretical elegance and appeal, string theory has not yet been experimentally verified.

1.1 Quantum corrections in GR

Pure classical GR in n dimensions is described in terms of the Einstein-Hilbert action which in natural units reads

$$S_{\text{EH}} = \frac{1}{16\pi G_n} \int d^n x \sqrt{-g} R + S_{\text{GHY}}$$

with S_{GHY} the standard Gibbons–Hawking–York boundary term that renders the variational problem well defined. G_n is the Newton constant in n dimensions, $g = \det(g_{\mu\nu})$ is the determinant of the spacetime metric, R is the Ricci scalar and we have assumed absence of matter fields. By construction, the Einstein-Hilbert action involves up to second order spacetime derivatives. In this sense, we can think of this

as the dominant term when the gravitational field is weak. In principle, nothing prevents us from modifying GR by adding higher derivatives terms in the action that respect the symmetries of our theory, which in this case are diffeomorphisms. For example, we could incorporate terms such as R^2 , $R_{\mu\nu}R^{\mu\nu}$ or $R_{\mu\nu\rho\sigma}R^{\mu\nu\rho\sigma}$. By dimensional analysis, we expect the respective couplings of these terms to be suppressed by some power of the Planck mass $M_P \equiv 1/\sqrt{16\pi G_n}$. Note that since these are all the possible terms which involve up to 4th order in spacetime derivatives they would become relevant in the strong field limit and negligible in the weak one. In fact, these types of corrections to the classical action arise naturally in some compactifications of string theories. This has precisely motivated several theories of modified gravity such as Chern-Simons or Gauss-Bonnet theory. In that sense, we could think of these additional terms as **quantum corrections** to the classical theory of gravity.

Continuing with this example, we could construct a general higher derivative gravity action up to the 4th order in spacetime derivatives, whose action in four dimensions would be:

$$S = S_{\text{EH}} + S_{\text{QC}} = \int d^4x \sqrt{-g} (M_P^2 R + \alpha R^2 + \beta R_{\mu\nu} R^{\mu\nu})$$

where α and β are dimensionless constants in natural units, and QC stands for quantum corrections. Note that we have not written the three possible scalar invariants explicitly since they are not independent by virtue of the Gauss-Bonnet theorem. In fact, this particular theory is renormalizable. Importantly, as we have previously remarked, we recover the standard Einstein-Hilbert term in the weak field limit, which is the one experimentally tested so far, as the higher derivative terms are negligible in that regime.

In this context, GR can be viewed as an effective theory of gravity, potentially requiring modifications at some cutoff scale, believed to be, as we have explained, around the Planck mass. This cutoff introduces the possibility of new physical phenomena emerging beyond this scale. Nevertheless, nature appears to conceal this regime from us, as horizons are expected to form whenever such scales become relevant. This phenomenon is encapsulated by the **Cosmic Censorship** (CC) conjecture in its weak form.

1.2 Cosmic censorship

Penrose proposed the CC conjecture suggesting that singularities arising from gravitational collapse are always obscured within event horizons of black holes, thereby preventing their direct observation from the external universe [52]. The conjecture exists in two formulations: the weak cosmic censorship conjecture posits that all singularities are shielded within event horizons, while the strong cosmic censorship conjecture states that, in most cases, timelike singularities do not occur, ensuring that even an observer entering a black hole will never witness the singularity [60]. This conjecture plays a pivotal role by averting the theoretical possibility of naked singularities, which would challenge fundamental principles of spacetime physics and black hole thermodynamics.

1.2.1 Cosmic censorship violation

We would like to answer the following question: *is it possible to violate the CC conjecture?* It turns out that the effort towards challenging or even violating the CC conjecture has been a topic of significant and longstanding interest in the scientific community. The main objective would require to dynamically generate spacetime regions with arbitrarily large curvature invariants without having to rely on fine tuned initial conditions. When such strong field spacetime regions emerge, the traditional Einstein-Hilbert action become inadequate as we have previously pointed out and some new physics must emerge. The ultimate aim is to produce a naked singularity from general enough initial conditions, indicating a breakdown of GR and the necessity of a new theory.

Nevertheless, violating CC in four-dimensional spacetimes is notoriously challenging, but there have been examples of this in higher dimensions [3, 29]. These examples often involve systems with Gregory-Laflamme (GL) instabilities. These are instabilities of certain black strings and black branes in dimensions higher than four. In particular, Gregory and Laflamme established that certain branes and higher-dimensional black string solutions in theories of gravity exhibit instabilities to small perturbations for dimensions $D \geq 5$ [36, 37]. Subsequent research into the endpoint of this instability has identified a critical dimension below which the instability results in a transition to a black hole phase. Specifically, for dimensions $5 \leq D \leq 13$, there are GL instabilities whereas for dimensions above the critical threshold, the instability leads to a non-uniform black ring phase [59].

The GL instabilities lead to the pinching off of the horizon in regions that are typically small, involving very low energies too as can be seen in Figure 1.1. This raises

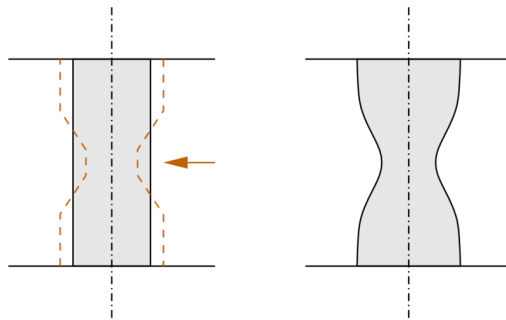


FIGURE 1.1: Pinching off of the horizon in a GL instability. Image taken from [50].

questions about the necessity of quantum gravity in understanding these processes, as they are often well-described by the large-D approximation of classical gravity [5, 4].

An analogy with a water stream helps explain why quantum effects might not be crucial in the horizon pinch-off. For thick streams, hydrodynamics provides a good approximation, whereas for thin streams, surface tension effects lead to drop formation, as can be seen in Figure 1.2. This mirrors the GL instability, where both the extended horizon (stream) and isolated black holes (drops) are adequately described by GR, revealing little about quantum gravity (molecular physics).



FIGURE 1.2: A water stream pinching off.

1.3 Goal of this thesis

The goal of this thesis is to present a mechanism that generates large curvatures in asymptotically anti-de Sitter (AdS) spacetimes in a boost invariant (BI) setup. In particular, we will provide solutions to Einstein-dilaton gravity in five dimensions where curvature corrections become dynamically significant over extended regions of spacetime. We are particularly interested in showing solutions where curvature invariants grow arbitrarily *everywhere* at the horizon, in contrast with GL instability. Consequently, even though we will find that a naked singularity will only appear in the infinite time limit in our system, curvature corrections to the action will become relevant within a finite amount of time given that the cutoff of GR is finite.

On the other hand, gauge/gravity duality, also known as AdS/CFT correspondence or holography, will prove to be a remarkable tool which will allow us to study the behaviour of a non-conformal strongly coupled plasma in terms of our gravitational solutions. This useful conjecture posits an equivalence between certain quantum field theories and gravitational theories in higher-dimensional anti-de Sitter (AdS) spaces. It suggests that a quantum field theory living on the boundary of an AdS space is dual to a gravitational theory in the bulk of the AdS space [51]. This duality provides a powerful tool for studying strongly coupled quantum field theories, where traditional perturbative methods may fail, by relating them to weakly coupled gravitational theories in higher dimensions. This correspondence has profound implications which are not yet fully understood, offering insights into topics ranging from black hole thermodynamics to the behavior of quark-gluon plasmas [2].

In our case, gauge/gravity will allow us to interpret our findings through fluid dynamics. In particular, the models we are going to consider are commonly used as holographic duals of QCD [40, 41, 42, 49]. We will see that the field theory interpretation of our gravitational system will be the following: the breakdown of classical gravity in the bulk will correspond to finite N and finite coupling corrections in the dual field theory. This reinforces the notion that a realistic and accurate holographic model of QCD must include stringy and quantum corrections.

1.4 Structure of this thesis

This thesis is structured as follows: Chapter 1 provides an introduction and rationale for the chosen topic. Chapter 2 explores gauge/gravity duality, which serves as the primary theoretical framework. Chapter 3 delves into the specific model under investigation, focusing on its thermodynamics and equilibrium transport properties. Chapter 4 introduces hydrodynamics and the boundary model, along with various plasma evolution scenarios. Chapter 5 presents dynamic solutions within our model, accompanied by results and their alignment with theoretical predictions. Chapter 6 discusses these findings within the context of the cosmic censorship conjecture. Finally, Chapter 7 presents the conclusions drawn from this study and outlines avenues for future research.

Chapter 2

The gauge/gravity duality

We are interested in computing properties of non conformal strongly coupled plasmas that are dual to our gravitational solutions. Nevertheless, computing observables in strongly coupled quantum field theories (QFTs) is notoriously difficult. In such cases, the interaction strength, described by the coupling constant, prevents the perturbative expansion of the generating functional since each successive term in the expansion is larger than the previous one. This issue does not arise in quantum electrodynamics (QED), where the coupling constant is small, allowing for successful perturbative calculations. However, quantum chromodynamics (QCD), the theory governing the interaction between quarks, is a prominent example of a strongly coupled QFT. To study such strongly coupled systems, new tools are required, one of which is the holographic principle or gauge/gravity duality.

In this chapter we provide a basic introduction to the gauge/gravity duality. We aim to cover the essential concepts, including a brief overview of string theory and the large N expansion of gauge theories, and we conclude with the famous conjecture that, in a certain limit, both partition functions are equal.

2.1 Introduction

As we have anticipated, gauge/gravity duality is a relationship between two types of physical theories, whose equivalence was first precisely conjectured by Juan Maldacena in 1997 [51]. It suggests a profound connection between string theory formulated in a higher-dimensional Anti-de Sitter (AdS) space and a conformal field theory (CFT) defined on the boundary of this space.

However, the initial idea originates from Gerard 't Hooft, who realized that non-Abelian strongly coupled $SU(N)$ gauge theories become extremely simplified when the number of colors is sent to infinity, $N \rightarrow \infty$ [1]. In the Feynman diagram representation, only the planar diagrams—those that can be drawn on a plane without crossings—are dominant in the large N limit. This insight laid the groundwork for the later development of the gauge/gravity duality, which provides a powerful toolkit for studying strongly coupled gauge theories using classical gravity.

2.2 All you need to know about string theory

String theory is a theoretical framework where point-like particles are replaced by one-dimensional objects known as strings. These strings can vibrate at different frequencies, with each vibrational mode corresponding to a different particle. In fact, strings can be either open or closed, with different boundary conditions leading to

different physical phenomena. Moreover, the theory is formulated in higher dimensions, typically ten in the case of superstring theory, which includes six compactified dimensions that are not observable at low energies.

There are five consistent superstring theories:

- Type I
- Type IIA
- Type IIB
- Heterotic SO(32)
- Heterotic E8 x E8

These theories are related by dualities. In particular, M-theory is a conjectured eleven-dimensional theory that unifies all five superstring theories. A crucial development in string theory was the discovery of D-branes, which are dynamical objects on which open strings can end. D-branes play a significant role in the gauge/gravity duality, as they provide a link between gauge theories and gravity [35, 53].

2.3 Anti-de Sitter spacetime

Anti-de Sitter (AdS) spacetime plays a fundamental role in the gauge/gravity duality. It is a maximally symmetric, negatively curved space that serves as the setting for the gravitational side of the correspondence. It can be visualized as a hyperboloid embedded in a higher-dimensional flat space. For example, AdS_{d+1} can be described by the surface:

$$-X_0^2 - X_{d+1}^2 + \sum_{i=1}^d X_i^2 = -L^2,$$

where L is the AdS radius, and the X 's are coordinates in a $(d+2)$ -dimensional flat space with metric

$$ds^2 = -dX_0^2 - dX_{d+1}^2 + \sum_{i=1}^d dX_i^2.$$

This embedding makes the symmetries of AdS space manifest, showing it has the isometry group $SO(2, d)$. A convenient coordinate system for AdS_{d+1} spacetime is the Poincaré coordinates, where the metric takes the form:

$$ds^2 = \frac{L^2}{z^2} (dz^2 + \eta_{\mu\nu} dx^\mu dx^\nu),$$

with $\eta_{\mu\nu}$ being the Minkowski metric in d -dimensions, and z is the radial coordinate with $z = 0$ corresponding to the boundary of AdS. The AdS spacetime has several important properties:

- **Boundary:** The boundary at $z = 0$ is a key feature since it is where the conformal field theory (CFT) lives.
- **Conformal Boundary:** The boundary of AdS is conformal to Minkowski space (or more generally, to a conformally flat space), which is why the dual theory on the boundary is a conformal field theory.

- **Curvature:** AdS space has a constant negative curvature, characterized by the AdS radius L .

2.4 The large N expansion

The large N expansion is a method used in quantum field theory and statistical mechanics to simplify the analysis of gauge theories by considering the limit where the number of colors, N , becomes very large. This technique was pioneered by Gerard 't Hooft in the 1970s [1]. In the large N limit, the gauge coupling constant g is rescaled such that $\lambda = g^2 N$, known as the 't Hooft coupling, remains constant. This parameter controls the perturbative expansion in the theory. In this limit, Feynman diagrams simplify significantly. The dominant contributions come from planar diagrams, which can be drawn on a plane without crossings. Non-planar diagrams are suppressed by factors of $1/N$, simplifying the analysis of the theory. The large N expansion plays a crucial role, as it provides a connection between the gauge theory on the boundary and the gravity theory in the bulk [62].

2.5 Gauge/gravity duality conjecture

As we have already anticipated, gauge/gravity duality posits a correspondence between a gravitational theory in a $d + 1$ dimensional AdS space and a conformal field theory on the d dimensional boundary of that space. The most studied example of this duality is the correspondence between Type IIB string theory on $AdS_5 \times S^5$ and $\mathcal{N} = 4$ supersymmetric Yang-Mills theory in four dimensions. In particular Maldacena's conjecture can be written as:

$$\left\langle e^{\int d^4x \phi_0(x^\mu) \mathcal{O}(x^\mu)} \right\rangle_{CFT} = \mathcal{Z}_{\text{string}} \left[\phi(x^\mu, z) \Big|_{z=0} = \phi_0(x^\mu) \right] \quad (2.1)$$

where $\phi(x^\mu, z)$ represents a scalar field (dilaton) in Anti-de Sitter space (AdS), with $\phi_0(x^\mu)$ serving as its boundary condition. This boundary condition acts as a source in the conformal field theory (CFT) for the scalar operator $\mathcal{O}(x^\mu)$ that is dual to the dilaton. This conjecture implies that any calculation in the strongly coupled CFT can be mapped to a weakly coupled gravity theory, and vice versa. This has been used to gain insights into various physical phenomena, including quark-gluon plasma, condensed matter systems, and black hole physics [61, 38, 2].

In conclusion, gauge/gravity duality represents a remarkable unification of concepts from string theory and gauge theory and a very powerful theoretical tool which we are going to use in this project to study strongly coupled systems using higher dimensional classical gravity solutions.

Chapter 3

The holographic model

In this chapter, we explain and motivate the model we will be working with on the gravity side, also referred to as the ‘bulk’. Additionally, we present numerical equilibrium solutions and show the thermodynamics and transport properties of the dual plasma.

3.1 The setup

We examine the dynamics and provide solutions for a five-dimensional holographic framework that couples gravity to a scalar field (the dilaton) possessing a non-trivial potential. Following the same conventions as in [6], the action for this Einstein-dilaton model is given by

$$S = \frac{2}{\kappa_5^2} \int d^5x \sqrt{-g} \left[\frac{1}{4} R - \frac{1}{2} (\nabla\phi)^2 - V(\phi) \right] + S_{GHY} \quad (3.1)$$

where S_{GHY} is the standard Gibbons–Hawking–York boundary term that renders the variational problem well defined. The resulting equations of motion are

$$R_{\mu\nu} - \frac{1}{2} R g_{\mu\nu} = 8\pi T_{\mu\nu} \quad (3.2)$$

$$\square\phi = \frac{\partial V}{\partial\phi}, \quad (3.3)$$

where the d’Alembertian operator in curved spacetime is $\square\phi = \frac{1}{\sqrt{-g}} \partial_\mu (\sqrt{-g} g^{\mu\nu} \partial_\nu \phi)$ and $\kappa_5^2 = \frac{8\pi G_5}{c^4}$ is the five-dimensional Einstein gravitational constant. The energy momentum tensor is defined as

$$8\pi T_{\mu\nu} = 2\partial_\mu\phi\partial_\nu\phi - g_{\mu\nu} \left[\frac{1}{2} g^{\alpha\beta} \partial_\alpha\phi\partial_\beta\phi + V(\phi) \right] \quad (3.4)$$

where the potential $V(\phi)$ encapsulates the characteristics of the dual gauge theory.

3.1.1 The potential

There are multiple options for choosing a potential. For specificity, we study a family of potentials defined by a single parameter γ . Let us consider the case where our potential can be expressed in terms of a simple superpotential:

$$W(\phi) = \frac{1 - 6\gamma^2 - \cosh(2\gamma\phi)}{4L\gamma^2} \quad (3.5)$$

where L is the AdS radius, such that

$$V(\phi) = -\frac{4}{3}W(\phi)^2 + \frac{1}{2}W'(\phi)^2. \quad (3.6)$$

If we explicitly write our potential as a function of ϕ we have that

$$V(\phi) = \frac{3\gamma^2 \sinh^2(2\gamma\phi) - 2(6\gamma^2 + \cosh(2\gamma\phi) - 1)^2}{24L^2\gamma^4}. \quad (3.7)$$

Interestingly, this potential is symmetric in ϕ and γ and has the particular feature that has a maximum at $\phi = 0$ and has no minimum, it is unbounded for $\gamma \in (0, \gamma_M = \sqrt{\frac{2}{3}})$. This can be seen in Figure 3.1. In fact, the behavior of the system at very

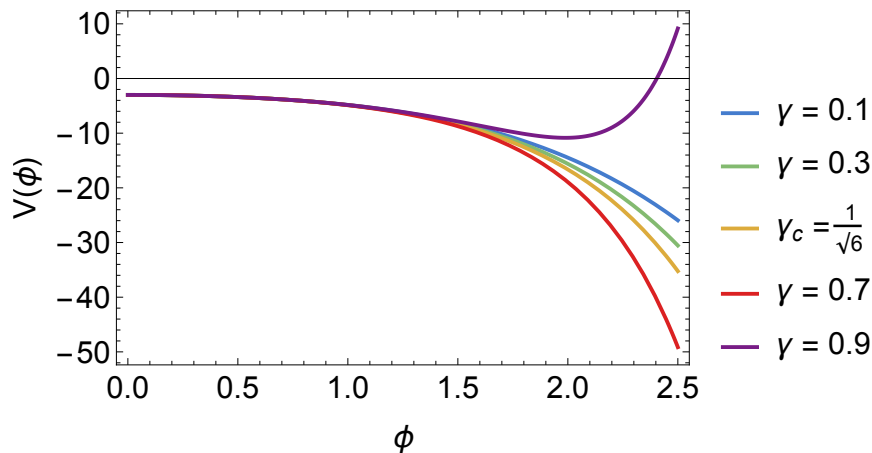


FIGURE 3.1: Our potential $V(\phi)$ for different choices of γ .

low energies is dominated by the leading exponential term for large values of ϕ , characterized by $V(\phi) \propto -e^{4\gamma\phi}$. Such runaway behavior is commonly observed in various string theory compactifications, including truncations of 10-dimensional supergravities (see, e.g., [30, 31, 25, 39]). Therefore, despite our initial choice of Eq. (3.6) as an exploratory model, we anticipate that our approach will yield similar outcomes in low-energy string theory scenarios in future studies. It is natural then to study the behaviour of the potential in the limits where the scalar field is near the maximum and when is rolling down the potential, which we can identify as the high and low energy limit respectively.

3.1.2 UV physics

In the UV limit, where $\phi \rightarrow 0$, the potential has a maximum at $\phi = 0$, as is clearly seen if we take the following limit

$$\lim_{\phi \rightarrow 0} V(\phi) = -\frac{3}{L^2}.$$

The fact that the maximum of the potential is at $-\frac{3}{L^2}$ is not arbitrary. At a technical level, the superpotential defined in Eq. (3.5) is selected to satisfy the following criteria:

- The vacuum solution is asymptotically AdS₅ in the UV characterised by a radius L , as $V(0) = -\frac{3}{L^2}$.

- The potential has a maximum at $\phi = 0$ and its second derivative indicates that the scalar field has a mass $m^2 = -\frac{3}{L^2}$ at that point. Consequently, in the UV regime, this field is dual to an operator \mathcal{O} in the gauge theory, possessing a dimension $\Delta_{UV} = 3$. Hence, $\phi = 0$ corresponds to a UV fixed point deformed by \mathcal{O} .
- There are not logarithmic terms in the UV expansion.
- The potential does not have phase transitions for $\gamma \in (0, \gamma_c)$, as discussed further in the subsequent sections.

It is also interesting to notice that even though the potential is not well defined for $\gamma = 0$, we can still compute the limit $\gamma \rightarrow 0$:

$$\lim_{\gamma \rightarrow 0} V(\phi) = \frac{1}{L^2} \left(-3 - \frac{3\phi^2}{2} - \frac{\phi^4}{3} \right). \quad (3.8)$$

We can do the same and explore the potential near the maximum where $\phi = 0$ and check that we cannot approximate the potential as an exponential but as a polynomial.

$$V(\phi) = \frac{1}{L^2} \left(-3 - \frac{3\phi^2}{2} - \frac{\phi^4}{3} - \left(\frac{2\gamma^2}{9} - \frac{4\gamma^4}{15} \right) \phi^6 + \mathcal{O}[\phi^8] \right). \quad (3.9)$$

Note on the conformal dimension Δ of an operator

The conformal (or scaling) dimension Δ of an operator is a measure of how the operator scales under conformal transformations, particularly under dilations (scaling transformations). In particular, an operator $\mathcal{O}(x)$ in a CFT is characterized by its behavior under a scaling transformation of the form:

$$x \rightarrow \lambda x$$

where λ is a positive scaling factor. The operator $\mathcal{O}(x)$ is said to have conformal dimension Δ if it transforms as:

$$\mathcal{O}(x) \rightarrow \lambda^{-\Delta} \mathcal{O}(\lambda x).$$

The conformal dimension Δ is an intrinsic property of the operator and plays a crucial role in determining the scaling behavior of correlation functions in the theory. For example, in d -dimensional Euclidean space, if $\mathcal{O}(x)$ is a primary operator, the two-point correlation function of \mathcal{O} typically takes the form:

$$\langle \mathcal{O}(x) \mathcal{O}(y) \rangle \propto \frac{1}{|x - y|^{2\Delta}}.$$

Therefore, the conformal dimension Δ dictates the power-law decay of the correlation function at large distances.

Note on the negative squared mass of the scalar field

It may be confusing that the scalar field possess negative squared mass. However, in AdS_{d+1} spacetimes one can identify the scalar field mass with the conformal dimension through:

$$m^2 L^2 = \Delta(\Delta - d).$$

As we can see in Figure 3.2, where we set $d = 4$, only the fields with $\Delta \geq 4$ will have $m^2 \geq 0$. On the other hand, the unitary bound imposes $\Delta \geq 1$. However, even though fields with scaling dimension $\Delta \leq 4$ will have negative squared mass, they are not always tachyons. The energy will be positive if and only if the Breitenlohner-Freedman bound $m^2 L^2 \geq -4$ is satisfied [16]. This is because the curvature contributes positively to the energy of the scalar field that is propagating through AdS.

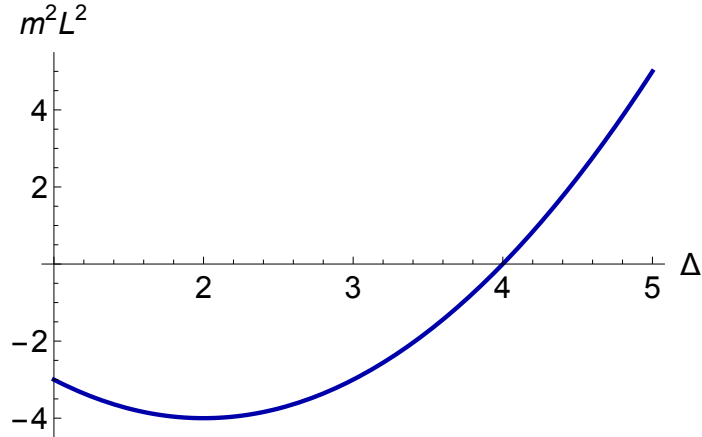


FIGURE 3.2: Scalar field mass as a function of the conformal dimension in AdS_5 .

3.1.3 IR physics

In the IR limit, where $\phi \rightarrow \infty$, the scalar field is rolling down the potential. We have already said that this potential has the particular feature that it is unbounded. Actually, the potential does not have a minimum for $\gamma < \gamma_M = \sqrt{\frac{2}{3}} \approx 0.816$. On the contrary, there will always be a minimum if $\gamma > \gamma_M$, as can be seen in Figure 3.1. This is clearly seen if we take the limit:

$$\lim_{\phi \rightarrow +\infty} V(\phi) = \begin{cases} +\infty & \text{if } \gamma > \sqrt{\frac{2}{3}} \\ -\infty & \text{if } 0 < \gamma < \sqrt{\frac{2}{3}} \end{cases}$$

It is also important to note that at late times/low energies the potential approaches an exponential:

$$V(\phi) \simeq \frac{(3\gamma^2 - 2) e^{4\gamma\phi}}{96L^2\gamma^4}, \quad \text{as } \phi \rightarrow +\infty \quad (3.10)$$

From here we can see that the potential resembles an exponential in this limit and goes to $\pm\infty$ depending on the value of γ . In fact, our results are primarily based on this runaway behavior. Importantly, we observe that stable black brane solutions exist even as ϕ increases, across a broad range of γ values. Drawing on this insight and the findings in [44], we anticipate that boost-invariant solutions will exhibit increasing curvatures at the horizon. In the next sections, we will demonstrate this explicitly by computing the full dynamical evolution. For values $\gamma > \gamma_M = \sqrt{\frac{2}{3}}$, we expect the theory to become pathological, as it will not have a maximum. This would correspond to a bad singularity according to [39].

3.2 Static Solutions

In this section we aim to explain how the equations of motion are numerically solved. We explain the procedure we follow in order to solve static black brane solutions in equilibrium. We have used *Mathematica* as a programming language.

To investigate the thermal properties of our model, we look for static black brane solutions of our action (3.1) using the same methodology as in [40, 6]. For these solutions, the scalar field acts as a monotonic function of the holographic coordinate z , allowing us to use it as a coordinate in solving the dynamic equations. The value of the scalar field at the black brane horizon, ϕ_H , uniquely determines the black brane solution. By applying the appropriate boundary conditions at various values of ϕ_H , one can compute all the equilibrium spacetime geometries. Determining the thermodynamics then involves finding a series of black brane solutions parameterized by ϕ_H , and calculating their Hawking temperatures T and entropy densities s .

3.2.1 The metric ansatz

We want to construct and examine the properties of black brane solutions of an asymptotically AdS_5 spacetime described by our action (3.1). A convenient ansatz in 5 dimensions written in Fefferman-Graham coordinates would be:

$$ds^2 = \frac{L^2}{z^2} (-f(z)dt^2 + g(z)d\vec{x}^2 + dz^2) \quad (3.11)$$

where z is the holographic radial coordinate, i.e. at the boundary $z = 0$ and grows in the bulk. Moreover, we have imposed the metric to be static in time and isotropic and homogeneous in the $\vec{x} = (x_1, x_2, x_3)$ coordinates. Therefore, the metric functions can only depend on z . The equations of motion can be simplified to a system of three second-order equations for f , g , and ϕ , along with a first-order constraint:

$$\begin{aligned} g'' &= \frac{9zg' - 2g(2V(\phi) + z^2\phi'^2 + 6)}{3z^2} \\ \phi'' &= \frac{-2g^2z^3\phi'^3 + 3g(zg' - 2g)\partial_\phi V(\phi) + z\phi'(g^2(4V(\phi) - 6) - 3z^2g'^2 + 9gzg')}{3gz^2(zg' - 2g)} \\ f'' &= f' \left(\frac{3}{z} - \frac{g'}{g} \right) + \frac{f'^2}{2f} + \frac{f(-4g^2(2V(\phi) + z^2\phi'^2 + 6) + z^2g'^2 - 4gz(zg'' - 3g'))}{2g^2z^2} \\ f' &= \frac{f(4g^2(-2V(\phi) + z^2\phi'^2 - 6) - 3z^2g'^2 + 18gzg')}{3gz(zg' - 2g)} \end{aligned}$$

where the prime derivative is just the derivative along z , i.e. $h' \equiv \frac{dh}{dz}$. We arranged them such that the equations for g and ϕ are independent of f , we have omitted the dependence of the functions with z and we have set $L = 1$.

3.2.2 Near boundary expansion

We solve the equations of motion perturbatively near the boundary, located at $z = 0$. We start by imposing the boundary metric to be conformally flat, as a boundary

condition. This allows us to know how the metric functions scale near the boundary:

$$f(z) = \sum_{n=0}^{\infty} f_n z^n, \quad g(z) = \sum_{n=0}^{\infty} g_n z^n \quad \text{and} \quad \phi(z) = \sum_{n=0}^{\infty} \phi_n z^{n+1}$$

and fixes the first coefficients to be

$$f_0 = 1 \quad \text{and} \quad g_0 = 1.$$

We can continue by solving the equations of motion order by order. The asymptotic expansions read:

$$\begin{aligned} f(z) &= 1 - \frac{\Lambda^2}{3} z^2 + f_4 z^4 + \mathcal{O}(z^6) \\ g(z) &= 1 - \frac{\Lambda^2}{3} z^2 + \left(\frac{2}{27} (\Lambda^4 - 9\Lambda\phi_v) - \frac{f_4}{3} \right) z^4 + \mathcal{O}(z^6) \\ \phi(z) &= \Lambda z + \phi_v z^3 + \mathcal{O}(z^5) \end{aligned}$$

where we have defined the source as $\Lambda \equiv \phi_0$ and the vacuum expectation value as $\phi_v \equiv \phi_2$. The coefficients f_4 , ϕ_0 and ϕ_2 are not determined by the expansions.

3.2.3 Near horizon expansion

To find black brane solutions, we require the existence of an event horizon at $z = z_H$. The suitable regularity conditions are

$$f(z) = f_H (z - z_H)^2 + \dots, \quad g(z) = g_H + \dots, \quad \phi(z) = \phi_H + \dots$$

Solving near horizon order by order we get:

$$\begin{aligned} f(z) &= f_H (z - z_H)^2 + \frac{f_H (z - z_H)^3}{z_H} + \mathcal{O}(z - z_H)^4 \\ g(z) &= g_H + \frac{2g_H (z - z_H)}{z_H} + \mathcal{O}(z - z_H)^2 \\ \phi(z) &= \phi_H + \frac{(z - z_H)^2 \sinh(2\gamma\phi_H) (-12\gamma^2 + (3\gamma^2 - 2) \cosh(2\gamma\phi_H) + 2)}{24\gamma^3 z_H^2} + \\ &\quad + \mathcal{O}(z - z_H)^3 \end{aligned} \tag{3.12}$$

3.2.4 Numerical integration

In order to numerically integrate the equations of motion we use the Mathematica's `NDSolve` routine and we take into account the following remarks:

- The equations of motion have a singular behavior at $z = z_H$, making it unsuitable to evaluate them at this point. Therefore, we use the expansions (3.12) computed to a sufficiently high order and evaluate them slightly away from the horizon at $z = z_H - \epsilon_H$. These results serve as the initial conditions for the functions and their derivatives. We start by assigning values to g_H , f_H , and ϕ_H . We begin with $f_H = L^{-2}$, $g_H = 1$, and $\phi_H = 10^{-2}$. Given the small value of ϕ_H , we expect to represent a high-temperature solution.
- Similarly, since the equations of motion are also singular at $z = 0$, we terminate the integration at a small value $z = \epsilon_{UV}$.

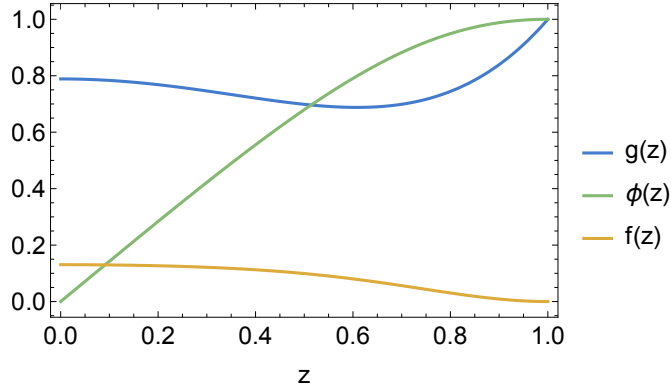


FIGURE 3.3: Solving the equations of motion by imposing $f_H = L^{-2}$, $g_H = 1$, and $\phi_H = 10^{-2}$ for $\gamma = 0.2$.

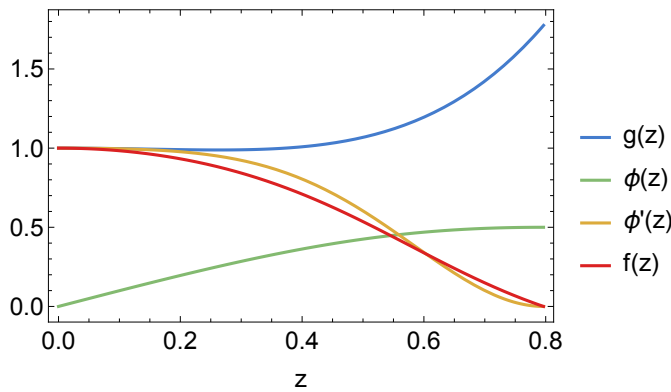


FIGURE 3.4: Solving the equations of motion by imposing that f_0 and g_0 approach unity in the UV region for $\gamma = 0.2$.

This is shown in Figure 3.3. From the numerical solution, we can extract the values f_0 , g_0 , and $\phi_s \equiv \Lambda$ from the asymptotic boundary solution. It is important to realize that there is a scaling symmetry in our ansatz of the following form:

$$\begin{aligned} f(z) &\rightarrow f'(z) = \alpha f(z) \\ g(z) &\rightarrow g'(z) = \beta g(z) \\ z &\rightarrow z' = \lambda z. \end{aligned}$$

Indeed, taking into account these isomorphisms of our ansatz, we adjust the values of f_H and g_H such that f_0 and g_0 approach unity in the UV region. In the same manner, we modify z_H so that the source $\phi_s = \Lambda$ remains constant across all solutions. This can be seen in Figure 3.4. With the near-boundary behavior now appropriately managed, we calculate the value of ϕ_v . Finally, we repeat this procedure for various values of $\phi_H \in (0, +\infty)$, which we can think of different values for the energy. For each resulting solution, we save the corresponding f_H , g_H , and ϕ_v . Finally, with these parameters, we can extract the thermodynamic information as we explain in the next section.

3.3 Thermodynamics

In this section we want to compute the thermodynamic quantities of our system. In particular, we will compute the pressure p , energy density ϵ , and free energy density f from the boundary data. Moreover, since black branes can be regarded as thermal systems we can extract its thermodynamic properties and relate them to the gauge theory dual. Specifically, the entropy density s and temperature T of an equilibrium state in the gauge theory side are related to the area density and surface gravity at the horizon of the corresponding black brane. We provide more detail about this in the next subsections where we set $c = \hbar = k_B = 1$.

3.3.1 Holographic renormalization

In this section we are going to follow the same approach as in [28, 6]. The idea is that the gravity and gauge theory partition function, as well as other observables, diverge near the boundary. By properly adding counterterms in the action that absorb these divergences, we are able to compute the pressure p , energy density ϵ , and free energy density f from the boundary information and relate them by using the standard thermodynamic relations

$$\epsilon + p = Ts \quad \text{and} \quad p = -f. \quad (3.13)$$

Noting the similarity between the small field behavior of the superpotential from (3.5) and the GPPZ flow in [34], we can straightforwardly determine the expectation values of the stress tensor and the scalar operator. Firstly, we expand the metric and the scalar field near the boundary in terms of the holographic coordinate z , i.e. in the limit where $z \rightarrow 0$. Following the approach in [10], we express the 5-dimensional metric for asymptotically AdS geometries in a general form using Fefferman-Graham coordinates:

$$ds^2 = \frac{L^2}{z^2} (dz^2 + g_{\mu\nu} dx^\mu dx^\nu)$$

and the asymptotic expansion for the metric and the scalar field read:

$$ds^2 = z^2 \left(g_{\mu\nu}^{(0)} + g_{\mu\nu}^{(2)} z^2 + g_{\mu\nu}^{(4)} z^4 + \dots \right), \quad (3.14)$$

$$\phi = \Lambda z + \phi_v z^3 + \dots \quad (3.15)$$

Therefore, using the results from [45], the expectation values of the field theory operators can be expressed as follows:

$$\langle T_{\mu\nu} \rangle = \frac{2L^3}{\kappa_5^2} \left(g_{\mu\nu}^{(4)} + \left(\Lambda \phi_v - \frac{\Lambda^4}{18} + \frac{\gamma^2 \Lambda^4}{24} \right) \eta_{\mu\nu} \right), \quad (3.16)$$

$$\langle O \rangle = -\frac{2L^3}{\kappa_5^2} \left(2\phi_v + \frac{\gamma^2 \Lambda^3}{6} \right). \quad (3.17)$$

As anticipated, equations (3.16) and (3.17) lead to the Ward identity for the trace of the stress tensor:

$$T^\mu_\mu = -\Lambda \langle O \rangle, \quad (3.18)$$

and we adopt a renormalization scheme where $\langle T_\mu^\nu \rangle = \langle O \rangle = 0$ in the vacuum. Hence, we will omit the expectation value notation and work with rescaled quantities:

$$\langle \epsilon, p_i, \mathcal{V} \rangle = \frac{\kappa_5^2}{2L^3} \langle -T_t^t, T_{x_i}^{x_i}, \mathcal{O} \rangle. \quad (3.19)$$

Now, we can write the thermodynamic quantities as a function of the boundary data:

$$\begin{aligned} \epsilon &= \frac{1}{72} (3\gamma^2 + 4) \Lambda^4 - f_4 - \Lambda\phi_v \\ p &= \frac{1}{216} \left((4 - 9\gamma^2) \Lambda^4 - 72f_4 + 72\Lambda\phi_v \right) \\ f &= \frac{1}{24} \left(\gamma^2 \Lambda^4 - \frac{3\sqrt{f_H g_H^3}}{z_H^3} - 12\Lambda\phi_v \right). \end{aligned}$$

In order to solve for f_4 , we realize that due to the symmetries of our equations of motion, there is a conserved charge Q along the holographic direction such that $\partial_z Q = 0$ where:

$$Q \equiv \frac{L^3}{z^3} \sqrt{\frac{g(z)}{f(z)}} (g(z)f'(z) - f(z)g'(z))$$

and evaluating the function at the boundary and at the horizon, allows us to compute f_4 :

$$f_4 = \frac{1}{18} \left(\Lambda^4 - 9\Lambda\phi_v \right) - \frac{3\sqrt{f_H g_H^3}}{8z_H^3}.$$

Finally, we obtain that:

$$\begin{aligned} \epsilon &= \frac{1}{24} \left(\gamma^2 \Lambda^4 + \frac{9\sqrt{f_H g_H^3}}{z_H^3} - 12\Lambda\phi_v \right) \\ p &= \frac{1}{24} \left(-\gamma^2 \Lambda^4 + \frac{3\sqrt{f_H g_H^3}}{z_H^3} + 12\Lambda\phi_v \right) \\ f &= \frac{1}{24} \left(\gamma^2 \Lambda^4 - \frac{3\sqrt{f_H g_H^3}}{z_H^3} - 12\Lambda\phi_v \right). \end{aligned}$$

3.3.2 Bekenstein-Hawking entropy

Bekenstein and Hawking [7] taught us that the entropy of a black brane can be computed as

$$S = \frac{A_H}{4G_N}$$

where A_H represents the "area" of the horizon (which corresponds to a volume in our context) and $G_N = \frac{\kappa_5^2}{8\pi}$ is the Newton constant in 5 dimensions. Given our ansatz for the bulk metric (3.11) the induced metric on the black brane horizon can be derived setting $dt = dz = 0$:

$$d\ell^2 = g_{ij} x^i x^j = \frac{L^2}{z^2} g(z) (dx_1^2 + dx_2^2 + dx_3^2).$$

The determinant of the induced metric tensor g_{ij} for the coordinates x_1, x_2 and x_3 is then:

$$\det(g_{ij}) = \frac{L^6}{z^6} g(z)^3$$

which allows us to compute the area element dA :

$$dA = \sqrt{\det(g_{ij})} dx_1 dx_2 dx_3 = \frac{L^3}{z^3} g(z)^{3/2} dx_1 dx_2 dx_3.$$

To find the total area, we should integrate this area element over the ranges of x_1, x_2 and x_3 :

$$\text{Area} = \frac{L^3}{z^3} g(z)^{3/2} \int dx_1 dx_2 dx_3.$$

Unfortunately, these coordinates are unbounded and the area diverges. In other words, we are not able to compute the total entropy because the total "area" of the horizon is infinite. Instead, we can actually compute the entropy density since we know the "area" density:

$$s = \frac{a_H}{4G_N} = \frac{L^3}{4G_N} \frac{g(z_H)^{3/2}}{z_H^3} = \frac{L^3}{4G_N} \frac{g_H^{3/2}}{z_H^3}$$

where we have used that $g(z_H) = g_H$ from the horizon expansion (3.12), $s = \frac{dS}{dx_1 dx_2 dx_3}$ is the entropy density and $a_H = \frac{dA}{dx_1 dx_2 dx_3}$ is the "area" density of the horizon.

3.3.3 Hawking Temperature

There exist various methods for calculating the Hawking temperature of a black brane. However, perhaps the most straightforward approach is to require smoothness of the Euclidean spacetime. This condition implies periodicity in imaginary time, which we can equate with the inverse temperature [18]. Let's begin by rewriting our general static black brane metric ansatz:

$$ds^2 = \frac{L^2}{z^2} (-f(z) dt^2 + g(z) d\vec{x} + dz^2) \quad (3.20)$$

where $f(z)$ and is assumed to have a second-order zero at the horizon $z = z_H$, while $g(z)$ remains non-zero there. Following the conventional approach [33], we perform a Wick rotation $t \rightarrow -it_E$ in order to get the Euclidean analytical continuation of the metric

$$ds_E^2 = \frac{L^2}{z^2} (f(z) dt_E^2 + g(z) d\vec{x} + dz^2). \quad (3.21)$$

Since we want to impose regularity at the horizon, we can expand our metric near the horizon $r \simeq r_H$:

$$ds_E^2 \simeq \frac{L^2}{z_H^2} \left(\frac{1}{2} f''(z_H) (z - z_H)^2 dt_E^2 + g(z_H) d\vec{x} + dz^2 \right). \quad (3.22)$$

Introducing radial and angular coordinates:

$$\rho = -\frac{L}{z_H}(z - z_H), \quad \theta = \sqrt{\frac{f''(z_H)}{2}} t_E \quad (3.23)$$

allows us to write the metric as

$$ds_E^2 \simeq d\rho^2 + \rho^2 d\theta^2 + g(z_H) d\vec{x}^2. \quad (3.24)$$

Notice that in these new coordinates the first two terms of the metric represent a plane in polar coordinates. Therefore, in order to avoid a conical singularity at $\rho = 0$ we must demand θ to have a periodicity of 2π . Moreover, from statistical field theory we know that Euclidean time is periodic with a periodicity of $\beta = \frac{1}{T}$. By equating both periods, we are left with an expression for the temperature of the black brane:

$$T = \frac{\sqrt{2f''(z_H)}}{4\pi} = \frac{\sqrt{f_H}}{2\pi} \quad (3.25)$$

where we have used that $f''(z_H) = 2f_H$ from the near horizon expansion (3.12). It is important to note that the Euclidean metric is not describing the spacetime inside the horizon $z > z_H$ since the origin of the polar coordinates is in the horizon itself.

3.4 Equation of state

The equation of state (EoS) of the dual theory can be computed from studying the properties of static black brane solutions to our action (3.1). Hence, the static solutions allows us to present the EoS in the form p/ϵ as a function of the energy density ϵ for different values of γ , as shown in Figure 3.5. The fact that p is positive for

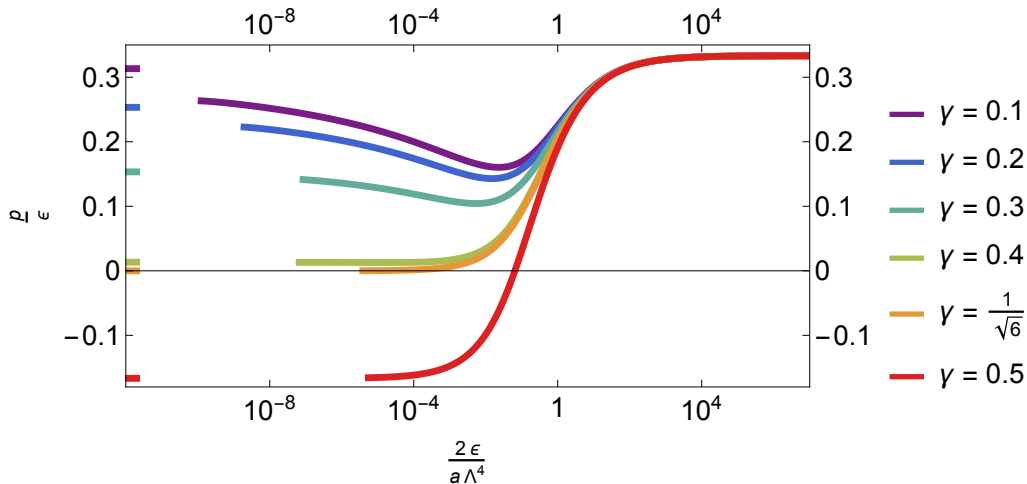


FIGURE 3.5: Equation of state for different values of $\gamma \in (0, \gamma_c]$ together with the low energy analytical prediction.

$\gamma \in (0, \gamma_c = \frac{1}{\sqrt{6}})$, indicates the absence of phase transitions in this range. On the contrary, for $\gamma > \gamma_c$ we see how the pressure becomes negative, indicating a phase transition. Following the work of [46], we use the coefficient of the Euler density appearing in the Weyl anomaly of the dual field theory $a = L^3/(2\pi G_5)$ to translate bulk to gauge theory quantities. Notice that at high energy we recover the equation

of state of a CFT $\frac{p}{\epsilon} = \frac{1}{3}$, that comes for the tracelessness of the energy momentum tensor. This is what we expect since our system is a CFT in the UV limit.

3.4.1 Low energy limit

In order to analytically compute the asymptotic equation of state (EoS) at low energies we are going to follow the same approach as [40]. There, the authors work with the same Einstein-dilaton theory, but with an exponential potential, which in our conventions reads:

$$V_G(\phi) = 4V_0 \exp(4\gamma\phi)$$

where the change of convention has been $\phi \rightarrow 2\phi$ and $V \rightarrow 4V$. We can also identify their potential parameter with our ($\gamma_G = 2\gamma$) in the limit where $\phi \rightarrow \infty$, since we can identify the Gubser potential with our potential in the low energy limit (3.10). In this subsection, we are going to work in this **low energy limit** $\phi \rightarrow +\infty$. The black brane static solutions describe the thermodynamics of the dual gauge theory via

$$\begin{aligned} \log s &= -\frac{\phi_H}{\gamma} + \text{constant in } \phi_H \\ \log T &= \left(2\gamma - \frac{1}{3\gamma}\right)\phi_H + \text{constant in } \phi_H. \end{aligned}$$

Since we know s and T

$$\begin{aligned} s(\phi_H) &= \exp\left(-\frac{\phi_H}{\gamma} + s_0\right) \\ T(\phi_H) &= \exp\left(\left(2\gamma - \frac{1}{3\gamma}\right)\phi_H + T_0\right) \end{aligned}$$

where s_0 and T_0 are constants in ϕ_H , we can compute the equation of state using

$$\begin{aligned} p(\phi_H) &= \int s dT = \frac{(6\gamma^2 - 1) e^{2\gamma\phi_H - \frac{4\phi_H}{3\gamma} + s_0 + T_0}}{6\gamma^2 - 4} \\ \epsilon(\phi_H) &= sT - p = \frac{3e^{2\gamma\phi_H - \frac{4\phi_H}{3\gamma} + s_0 + T_0}}{4 - 6\gamma^2}. \end{aligned}$$

We can now take the ratio of p and ϵ to get the equation of state

$$\boxed{\frac{p}{\epsilon} = \frac{1}{3} - 2\gamma^2}. \quad (3.26)$$

Notice that in the high temperature limit, where $\gamma \rightarrow 0$ we recover the usual $1/3$ since the system approaches a CFT and the pressure starts to be negative at precisely $\gamma_c = \frac{1}{\sqrt{6}}$, indicating a phase transition. Interestingly, we can compare the predicted equation of state from (3.26) for different choices of γ with the numerical results and check that they match at low energies. This is shown in Figure 3.5. We can also plot the behaviour of the equation of state in the low energy limit (3.26) for different values of γ . This can be seen in Figure 3.6.

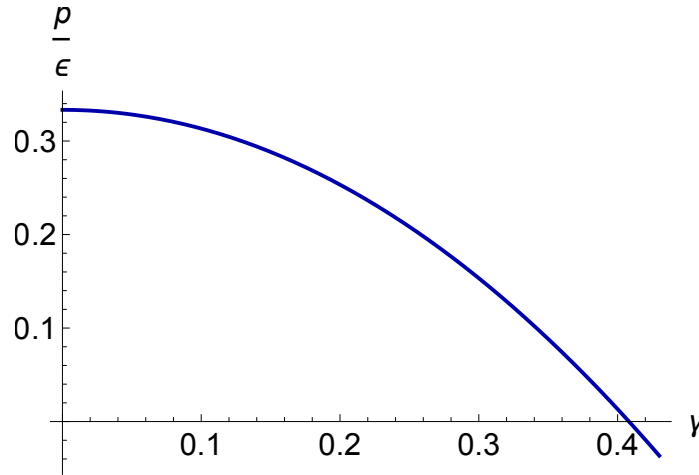


FIGURE 3.6: Predicted analytical behaviour of the equation of state at low energies as a function of γ .

3.4.2 Equation of state for different γ 's

For completeness, we also illustrate the behavior of the energy density as a function of temperature for three values of γ in distinct qualitative regimes in Figure 3.7.

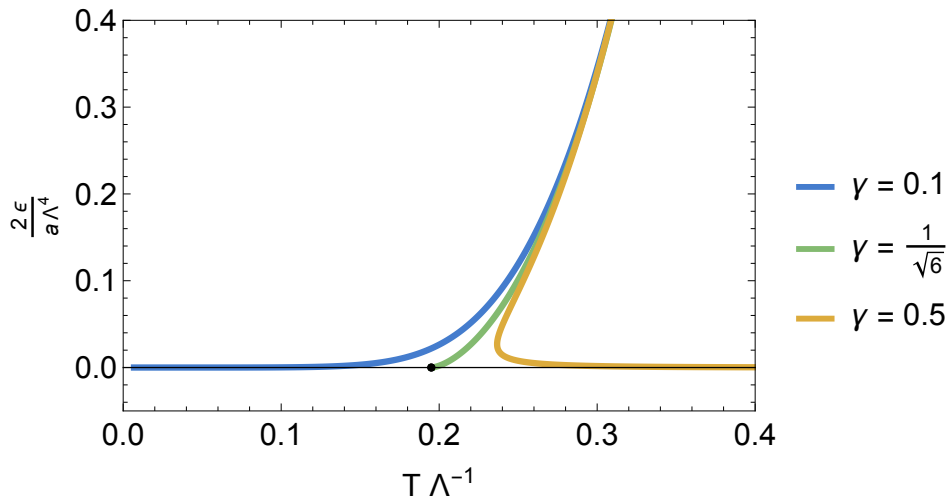


FIGURE 3.7: Energy density as a function of the temperature for $\gamma = 0.1, 1/\sqrt{6}, 0.5$.

Note that for $0 < \gamma < \gamma_c$, the energy smoothly approaches zero as the temperature decreases. In the limiting case $\gamma_c = 1/\sqrt{6} \simeq 0.408$, the temperature asymptotically reaches a constant value as the energy vanishes, consistent with the results of [43, 26, 8]. Above this value, there is an energy threshold below which homogeneous black branes become unstable, leading to a phase transition. Finally, when $\gamma > 2\gamma_M = \sqrt{2/3}$, the theory is expected to exhibit pathological behaviour, as discussed in [39]. To understand this better we plot the free energy density for the same values of γ in Figure 3.8. There we see how the free energy density becomes positive, and thus unstable for $\gamma > \gamma_c = 1/\sqrt{6}$, indicating the presence of a phase transition.

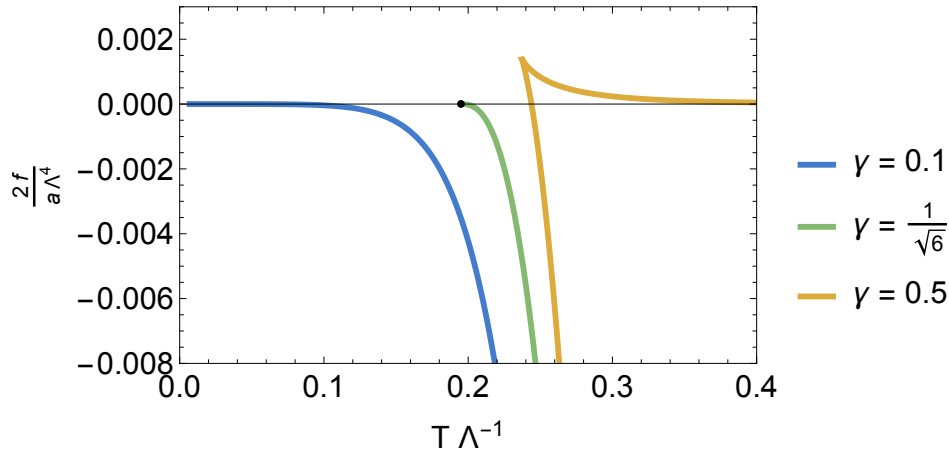


FIGURE 3.8: Free energy density as a function of the temperature for $\gamma = 0.1, 1/\sqrt{6}, 0.5$.

3.5 Transport coefficients

The static solutions also enables us to compute transport coefficients. Specifically, the shear and bulk viscosities are given by [54, 27]

$$\frac{\eta}{s} = \frac{1}{4\pi}, \quad \frac{\zeta}{\eta} = 4 \left(\frac{\partial \log s}{\partial \phi_H} \right)^{-2}, \quad (3.27)$$

where ϕ_H is the value of the scalar ϕ at the horizon. The bulk over shear viscosity ratio is shown in Figure 3.9.

3.5.1 Low energy limit

In order to compute the bulk to shear viscosity ratio and the speed of sound analytically in the low energy limit, we follow again the same approach as [40]. Using the relation between static solutions and fluid properties provided in [6], we can explore how the thermodynamics variables asymptotically behaves as a function of our γ :

$$\lim_{\phi \rightarrow +\infty} \frac{\zeta}{\eta} = 4\gamma^2$$

and check that perfectly matches the low energy behaviour of the numerical values for the bulk to shear viscosity ratio. The results can be seen from Figure 3.9. In the same way, we can also get the speed of sound c_s :

$$c_s^2 = \frac{d \log T}{d \log s} = \frac{1}{3} - 2\gamma^2$$

which in the limit where $\phi \rightarrow +\infty$ indicates a phase transition at

$$\gamma_c = \frac{1}{\sqrt{6}} \approx 0.408$$

that coincides with the numerical critical value as it can be seen in Figure 3.7.

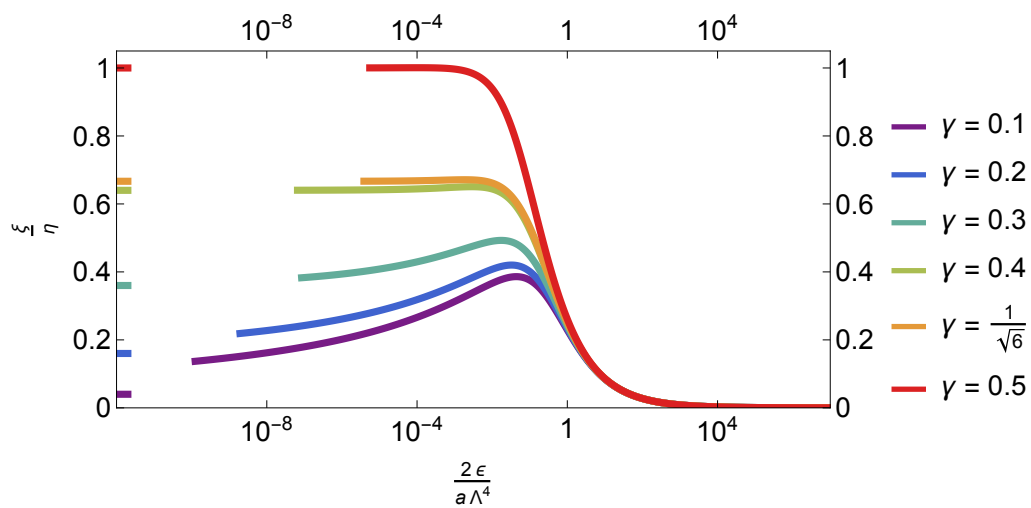


FIGURE 3.9: Bulk to shear viscosity ratio as a function of the energy density for $\gamma = 0.1, 0.2, 0.3, 0.4, 1/\sqrt{6}$ together with the low energy analytical prediction.

Chapter 4

Hydrodynamics and quark-gluon plasma

Until now, we have been discussing the "bulk" or gravity model. In this chapter, we want to describe the boundary model, where the strongly coupled quantum field theory lives. In particular, we aim to model the behavior of the quark-gluon plasma (QGP) produced in heavy ion collisions. QGP is a unique phase of quantum chromodynamics (QCD) in which quarks and gluons, the fundamental constituents of protons and neutrons, are no longer confined within individual nucleons but instead exist in a free, deconfined state. This phase occurs at extremely high temperatures and energy densities, similar to those that existed in the universe shortly after the Big Bang. It turns out that the cooling of the QGP is well described by hydrodynamics from very early times. Therefore, we will explain hydrodynamics and explore different types of energy flows.

4.1 Dynamics of relativistic collisions

We are interested in studying relativistic head on collisions. Let us assume the collision axis to be in the z direction. Since we want to simulate relativistic heavy ions that travel very close to the speed of light, it is not convenient to work with standard coordinates such as t and z since distances Δt , Δz are not invariant under Lorentz transformations. In fact, in this relativistic set up it is more appropriate to work with the so called Milne coordinates, i.e. proper time τ and spacetime rapidity y defined as:

$$\begin{aligned}\tau &= \sqrt{t^2 - z^2} \\ y &= \operatorname{arctanh} \frac{z}{t} = \frac{1}{2} \log \frac{t+z}{t-z}\end{aligned}\tag{4.1}$$

due to the fact that under a boost along the collision direction z , proper time remains invariant whereas the rapidity y is additive, i.e. it will be shifted by a constant [47]. In Figure 4.1 we can schematically see the relativistic head-on collision in the (z, t) plane. Where the hyperbolas are constant proper time slices and the red line represents constant rapidity. Therefore, in order to write our metric in the new coordinates we can invert the relations in 4.1 to obtain $t(\tau, y)$ and $z(\tau, y)$:

$$\begin{aligned}t &= \tau \cosh y \\ z &= \tau \sinh y.\end{aligned}\tag{4.2}$$

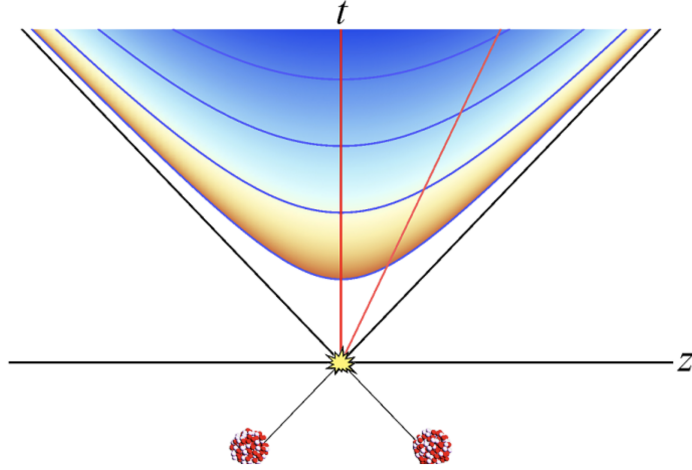


FIGURE 4.1: Relativistic heavy ion head-on collision in the (z, t) plane. Image taken from [57]. The red lines represent constant rapidities y whereas the hyperbolas are lines of constant proper time τ .

4.1.1 A model for quark-gluon plasma

The strongly coupled quantum field theory that we want to holographically study lives in the boundary of an asymptotic AdS_5 spacetime. Since we are interested in modelling heavy ion collisions, we are going to impose for the boundary spacetime to be flat, i.e. described by a Minkowski metric in four dimensions:

$$ds_B^2 = \gamma_{\mu\nu} dx^\mu dx^\nu = -dt^2 + dz^2 + dx_1^2 + dx_2^2.$$

As we have seen, it is natural to consider the proper time τ and the rapidity y for head-on heavy ion collisions. Considering z to be the colliding direction and using the change of coordinates (4.2), the boundary metric in these coordinates is given by the so called Milne metric [58]:

$$ds_B^2 = -d\tau^2 + \tau^2 dy^2 + dx_1^2 + dx_2^2. \quad (4.3)$$

From now on, we will follow the heavy ion collision model proposed by Bjorken [12], where we assume the collision to be boost invariant in the central rapidity region along the colliding direction z . This means that physical quantities will be independent of the rapidity y . We will also assume rotational symmetry in the transverse plane (x_1, x_2) which implies that our physical observables will only depend on the proper time τ . Finally, we work in the fluid rest frame where τ is the proper time of the fluid so the four velocity is just $u^\mu = \partial/\partial\tau$.

In the following sections, we will delve deeper into the hydrodynamic description of this system and present both analytical and numerical results, highlighting the behavior of the system under various conditions.

4.2 Hydrodynamics

In the context of gauge/gravity duality, the study of hydrodynamics provides crucial insights into the behavior of strongly coupled quantum field theories. Hydrodynamics describes the macroscopic behavior of fluids and is characterized by conserved quantities such as energy, momentum, and charge densities. In our setup, we focus on the hydrodynamics of a strongly coupled quantum plasma which may have similar properties as the quark-gluon plasma, a state of matter produced in heavy-ion collisions.

The fundamental equations governing hydrodynamics are the conservation laws of the energy-momentum tensor $T^{\mu\nu}$, given by $\nabla_\mu T^{\mu\nu} = 0$. To first order in a gradient expansion of the fluid four-velocity, the energy-momentum tensor can be expressed as

$$T^{\mu\nu} = \epsilon u^\mu u^\nu + p \Delta^{\mu\nu} - \eta \sigma^{\mu\nu} - \zeta \Delta^{\mu\nu} \nabla_\lambda u^\lambda \quad (4.4)$$

where ϵ is the energy density, p is the pressure, η is the shear viscosity, ζ is the bulk viscosity, and u^μ is the fluid velocity in some particular reference frame. The shear tensor $\sigma^{\mu\nu}$ is defined as

$$\sigma^{\mu\nu} = \Delta^{\mu\alpha} \Delta^{\nu\beta} (\nabla_\alpha u_\beta + \nabla_\beta u_\alpha) - \frac{2}{3} \Delta^{\mu\nu} \nabla_\lambda u^\lambda \quad (4.5)$$

while the projector tensor $\Delta^{\mu\nu} = \gamma^{\mu\nu} + u^\mu u^\nu$ projects onto the space transverse to the fluid velocity. Here, $\gamma_{\mu\nu}$ is the metric, which in our case will be flat and expressed in boost-invariant coordinates. This choice is particularly useful for modeling the cooling of the quark-gluon plasma produced in heavy-ion collisions [12] as we have explained in the previous section.

Let us assume that the gauge theory matter behaves like a perfect fluid plus 1st order hydro as described in (4.4). By explicitly writing the components of the energy momentum tensor:

$$T^{\mu\nu} = \begin{pmatrix} \epsilon(\tau) & 0 & 0 & 0 \\ 0 & \frac{-3\zeta(\tau) - 4\eta(\tau) + 3\tau p(\tau)}{3\tau^3} & 0 & 0 \\ 0 & 0 & \frac{2\eta(\tau) - 3\zeta(\tau)}{3\tau} + p(\tau) & 0 \\ 0 & 0 & 0 & \frac{2\eta(\tau) - 3\zeta(\tau)}{3\tau} + p(\tau) \end{pmatrix}$$

we can identify the hydrodynamic predictions for both the longitudinal and transverse pressures using:

$$T^{\mu}_{\nu} = \text{diag}(-\epsilon, p_{\parallel}, p_{\perp}, p_{\perp}) . \quad (4.6)$$

Therefore, we have that:

$$p_{\parallel}(\tau) = p(\tau) - \frac{3\zeta(\tau) + 4\eta(\tau)}{3\tau} \quad (4.7)$$

$$p_{\perp}(\tau) = p(\tau) + \frac{2\eta(\tau) - 3\zeta(\tau)}{3\tau} . \quad (4.8)$$

The energy momentum tensor conservation provides us with a simple first order differential equation for the energy density of the following form:

$$\nabla_\mu T^{\mu\nu} = 0 \quad \rightarrow \quad \epsilon'(\tau) = \frac{\zeta(\tau) + \frac{4\eta(\tau)}{3} - \tau p(\tau) - \tau \epsilon(\tau)}{\tau^2} \quad (4.9)$$

which can be written in terms of the longitudinal pressure as

$$\boxed{\tau\epsilon'(\tau) + \epsilon(\tau) + p_{\parallel}(\tau) = 0}. \quad (4.10)$$

We are now going to study the solutions to this equation for different scenarios, i.e. different flows for the energy density as a function of proper time.

4.3 Ideal Bjorken flow

Let us suppose that the gauge theory matter is conformal and behaves as a perfect fluid. This is what we call an ideal Bjorken flow. Therefore, its energy momentum tensor will be of the form:

$$T_{\mu\nu} = (\epsilon + p)u_{\mu}u_{\nu} + p\eta_{\mu\nu}$$

where ϵ is the energy density, p is the pressure and u^{μ} is the fluid local four-velocity, with $u^2 = -1$. In our coordinates (τ, y, x_1, x_2) , the fact that we consider a boost-invariant set up implies that $u^{\mu} = (1, 0, 0, 0)$ and the energy momentum tensor reads:

$$T_{\mu\nu} = \begin{pmatrix} \epsilon(\tau) & 0 & 0 & 0 \\ 0 & \tau^2 p(\tau) & 0 & 0 \\ 0 & 0 & p(\tau) & 0 \\ 0 & 0 & 0 & p(\tau) \end{pmatrix} \quad (4.11)$$

Since we are considering a conformal case, the energy momentum tensor should be traceless. This relations gives us the equation of state

$$T_{\mu}^{\mu} = 0 \rightarrow p(\tau) = \frac{\epsilon(\tau)}{3}. \quad (4.12)$$

Moreover, the conservation of the energy momentum tensor gives us an extra condition.

$$\nabla_{\mu} T^{\mu\nu} = 0 \rightarrow \epsilon'(\tau) = -\frac{p(\tau) + \epsilon(\tau)}{\tau} \quad (4.13)$$

Solving (4.13) for $E(\tau)$ using the EoS (4.12) allows us to compute analytically how the energy density evolve with proper time if the matter theory behave like an ideal fluid:

$$\boxed{\epsilon(\tau) = \frac{\epsilon_0}{\tau^{4/3}}} \quad (4.14)$$

where $\epsilon_0 = \tau_0^{4/3}\epsilon(\tau_0)$. Note that it is necessary to have an equation of state relating energy and pressure in order to close the system of equations and get a solution. From (4.14) we can extract how the thermodynamic quantities evolve with proper time [32]:

$$\begin{aligned} \epsilon, p &\sim \tau^{-4/3} \\ T &\sim \epsilon^{1/4} \sim \tau^{-1/3} \\ s &\sim T^3 \sim \tau^{-1} \\ sV &\sim s\tau \sim \text{const.} \end{aligned}$$

Let us generalize Bjorken flow by studying the **non-conformal** case for an ideal fluid and with first order hydrodynamic corrections.

4.4 Ideal non-conformal Bjorken flow

In this section we study the non-conformal behaviour of the energy density as a function of proper time, assuming that our gauge theory matter is described by an ideal fluid. In order to analytically solve the energy momentum tensor conservation equation we need an equation of state. The problem is that for non conformal theories with a non trivial potential for the scalar field like the one in our model, is very hard to find analytical solutions.

Fortunately our potential at late times behaves as an exponential (3.10) and there exist analytical black brane solutions with these kind of potentials in the literature. In particular, in order to study the late time behaviour of our non-conformal plasma as a function of proper time, we are going to follow the same approach as in [44]. In this paper the authors studied the thermalization of $N = 4$ SYM plasmas holographically and found analytical black brane solutions to the same action as us (3.1) but with an exponential potential for the scalar field of the form:

$$V(\phi) = 2V_0 (3\gamma^2 - 2) e^{4\gamma\phi}. \quad (4.15)$$

where the change of conventions between their action and ours is $\phi \rightarrow \sqrt{3/2}\phi$ and $V \rightarrow -4V$. Importantly, this theory can be mapped to ours at low energies $\phi \rightarrow +\infty$, since the scalar field is rolling down a potential which is effectively exponential as we have shown in (3.9).

Notice that in their original expression for the potential they work with a parameter called X , which is related to our γ . Indeed, we can compare their potential with our potential at late times and match the exponents in order to get a map between both theories $X = -\sqrt{\frac{3}{2}}\gamma$. This parameter represents a conformality factor, i.e. it measures how one deviates from the conformal case. In fact, if one send $\gamma \rightarrow 0$ in their theory, one recovers the conformal case.

Nevertheless, in our case this is not exactly the same since sending $\gamma \rightarrow 0$ does not imply a recovering of conformality as it can be seen from (3.8). This is because we impose AdS in the boundary while they do not, since they only care about the IR. In fact, it is clear from their potential that they do not have an stable vacuum and thus the theory is not well defined in the UV, requiring a UV completion.

Remarkably, they found an analytical black brane solution in a boost invariant setup in the same fashion as in [48] but generalizing to the non-conformal case.

4.4.1 Black brane solution

In our conventions, the general analytical solution for (3.1) with the scalar field potential (4.15) found in [44] at leading order in $1/\tau$ and in the IR limit is

$$ds^2 \simeq v^{\frac{2}{6\gamma^2-1}} \left\{ \frac{\tau^{-4\gamma^2}}{1-v^\xi} dv^2 + \tau^{-\frac{2}{3}} \left[-(1-v^\xi)d\tau^2 + \tau^2 dy^2 + dx_\perp^2 \right] \right\} \quad (4.16)$$

and the solution for the scalar field reads

$$e^\phi = \tau \sqrt{\frac{3}{2}} \gamma v \frac{3\sqrt{\frac{3}{2}}\gamma}{1-6\gamma^2}$$

where we defined the scaling variable v as

$$v = \frac{z}{\tau^{\frac{1}{3}-2\gamma^2}}$$

and z is the holographic coordinate. Moreover, we work in the gauge where:

$$\xi = \frac{3}{1-6\gamma^2} + 1. \quad (4.17)$$

In fact, the metric (6.2) is nothing but a black hole solution with moving horizon. This is clearer when we express the metric as a function of z using (6.1) at leading order in $1/\tau$:

$$ds^2 \simeq z^{\frac{2}{6\gamma^2-1}} \left\{ \frac{dz^2}{1-\tau^2\gamma^2-\frac{4}{3}z^\xi} - \left(1-\tau^2\gamma^2-\frac{4}{3}z^\xi\right) d\tau^2 + \tau^2 dy^2 + dx_\perp^2 \right\} \quad (4.18)$$

and the scalar field reads:

$$e^\phi = z \frac{3\sqrt{\frac{3}{2}}\gamma}{1-6\gamma^2}.$$

4.4.2 Late time thermodynamics

From the black brane solution (6.4) we can compute the thermodynamics in the same manner as in [44], where they have assumed that the gauge theory matter is described by an ideal fluid, at late times as a function of γ and τ :

$$\begin{aligned} T(\tau) &= \frac{(2-3\gamma^2)}{2\pi} \tau^{2\gamma^2-\frac{1}{3}} \sim \tau^{2\gamma^2-\frac{1}{3}} \\ s(\tau) &= \frac{1}{4G_5} \tau^{-1} \sim \tau^{-1} \\ \epsilon(\tau) &= \frac{3}{16\pi G_5} \tau^{2\gamma^2-\frac{4}{3}} \sim \tau^{2\gamma^2-\frac{4}{3}} \\ F(\tau) &= \frac{(6\gamma^2-1)}{16\pi G_5} \tau^{2\gamma^2-\frac{4}{3}} \sim \tau^{2\gamma^2-\frac{4}{3}} \\ p(\tau) &= \frac{(1-6\gamma^2)}{16\pi G_5} \tau^{2\gamma^2-\frac{4}{3}} \sim \tau^{2\gamma^2-\frac{4}{3}}. \end{aligned} \quad (4.19)$$

Note that the entropy density is for the volume element $\tau dy dx_1 dx_2$. Looking at (4.19), it is clear from the free energy and the pressure that there is a phase transition at $\gamma_c = \frac{1}{\sqrt{6}}$. Indeed, when $\gamma > \gamma_c = \frac{1}{\sqrt{6}}$ the free energy becomes positive and the pressure becomes negative, indicating the instability of the solution. Moreover, the temperature becomes negative at $\gamma_M = \sqrt{\frac{2}{3}}$ since the potential (4.15) changes its sign, preventing the rolling of the scalar field.

Importantly, we have found that the non conformal behaviour for the energy density

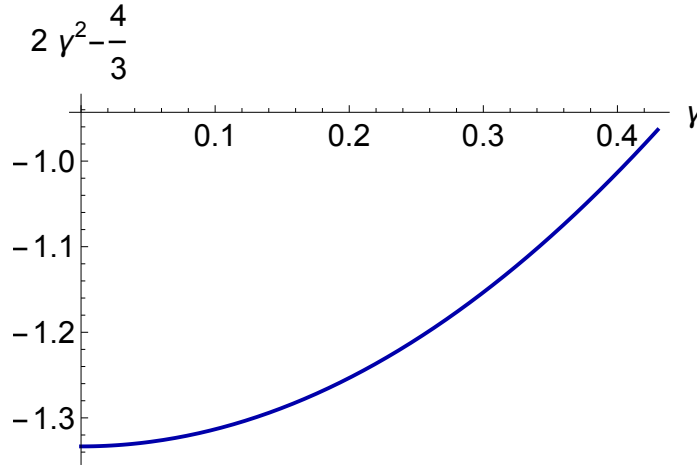


FIGURE 4.2: Non conformal exponent of the energy density flow described by an ideal fluid as a function of γ .

of the quantum fluid in the ideal case is described by the exponent:

$$\boxed{\epsilon(\tau) \sim \tau^{2\gamma^2 - \frac{4}{3}}}. \quad (4.20)$$

Notice that in the case where $\gamma = 0$ we recover the usual Bjorken flow, i.e. $\epsilon(\tau) \sim \tau^{-4/3}$. In fact, as we can see from (4.20), **the larger γ is the slower the energy evolves** as we can see in Figure (4.2). We have worked in the same units as the authors and written the pre-factors taking into account that they depend on the whole background which is different from ours in the UV thus some correction is needed, but we can expect the exponent of τ to be correct. As a nice check, we see that we recover the same equation of state as in (4.12) once we divide the pressure by the energy density:

$$\frac{p(\tau)}{\epsilon(\tau)} = \frac{1}{3} - 2\gamma^2.$$

4.5 Viscous corrections to non-conformal Bjorken flow

Let us assume that the gauge theory matter behaves like a perfect fluid plus 1st order hydro. Following the same approach as in [40], which we already started in section 3.4.1, we compute the thermodynamics as a function of ϕ_H :

$$\begin{aligned} T(\phi_H) &= T_0 e^{2(\gamma - \frac{1}{6\gamma})\phi_H} \\ s(\phi_H) &= s_0 e^{-\frac{\phi_H}{\gamma}} \\ p(\phi_H) &= \frac{(6\gamma^2 - 1)s_0 T_0}{6\gamma^2 - 4} e^{2\gamma\phi_H - \frac{4\phi_H}{3\gamma}} \\ \epsilon(\phi_H) &= \frac{3s_0 T_0}{4 - 6\gamma^2} e^{2\gamma\phi_H - \frac{4\phi_H}{3\gamma}} \end{aligned}$$

where T_0 and s_0 are constants in ϕ_H fixed by our theory. As a preliminary step, we assume the very late-time behavior from (3.26) and write every term in (4.9) as a

function of the energy density using:

$$\begin{aligned}\zeta(\tau) &= 4\gamma^2\eta(\tau) \\ p(\tau) &= \left(\frac{1}{3} - 2\gamma^2\right)\epsilon(\tau) \\ \eta(\tau) &= \frac{s(\tau)}{4\pi} \\ s(\tau) &= 3^{\frac{3}{6\gamma^2-4}}s_0 \left(\frac{(4-6\gamma^2)\epsilon(\tau)}{s_0T_0}\right)^{\frac{3}{4-6\gamma^2}}\end{aligned}$$

resulting in a rather complicated first order ordinary differential equation for the energy of the form:

$$\boxed{A_\gamma\epsilon'(\tau) + B_\gamma\frac{\epsilon(\tau)}{\tau} + C_\gamma\frac{\epsilon(\tau)^{\frac{3}{4-6\gamma^2}}}{\tau^2} = 0} \quad (4.21)$$

where the coefficients are:

$$\begin{aligned}A_\gamma &= -3 \\ B_\gamma &= 2(3\gamma^2 - 2) \\ C_\gamma &= \frac{2^{\frac{3}{4-6\gamma^2}}3^{\frac{3}{6\gamma^2-4}}(2-3\gamma^2)^{\frac{3}{4-6\gamma^2}}(3\gamma^2+1)\Sigma_0}{\pi}\end{aligned}$$

and we have defined $\Sigma_0 = T_0(s_0T_0)^{-\frac{3}{4-6\gamma^2}}$ for notation simplicity. Notice that we can identify $C_\gamma\frac{\epsilon(\tau)^{\frac{3}{4-6\gamma^2}}}{\tau^2}$ as the **viscous term**, since it carries all the information from hydro. It is important to realize that it is suppressed by a factor of τ^{-2} . One way of seeing this is the following. If we send this term to 0, and we solve the differential equation (4.21), we recover:

$$\epsilon(\tau) = \epsilon_0\tau^{2\gamma^2-\frac{4}{3}}$$

which is precisely the non-conformal ideal case (4.20) discussed in the previous section. Therefore, it is clear that the viscous term is the one carrying information about the hydrodynamics.

Let's first analyse the solution of (4.21) for the extreme cases where $\gamma = 0$ and $\gamma_c = \frac{1}{\sqrt{6}}$ in order to gain some intuition:

$$\begin{aligned}\epsilon(\tau)|_{\gamma=0} &= \left(\frac{c_1}{\tau^{1/3}} - \frac{c_2}{\tau}\right)^4 \\ \epsilon(\tau)|_{\gamma=\frac{1}{\sqrt{6}}} &= \frac{\epsilon_0 e^{-\frac{\Sigma_0}{2\pi\tau}}}{\tau}\end{aligned}$$

where c_1 is a constant of integration and we have defined $c_2 = \frac{\Sigma_0}{2\sqrt{2}3^{3/4}\pi}$. Again, we can identify $\frac{c_2}{\tau}$ as the hydro correction or viscous term which at late times is clearly negligible compared with the ideal one $\frac{c_1}{\tau^{1/3}}$.

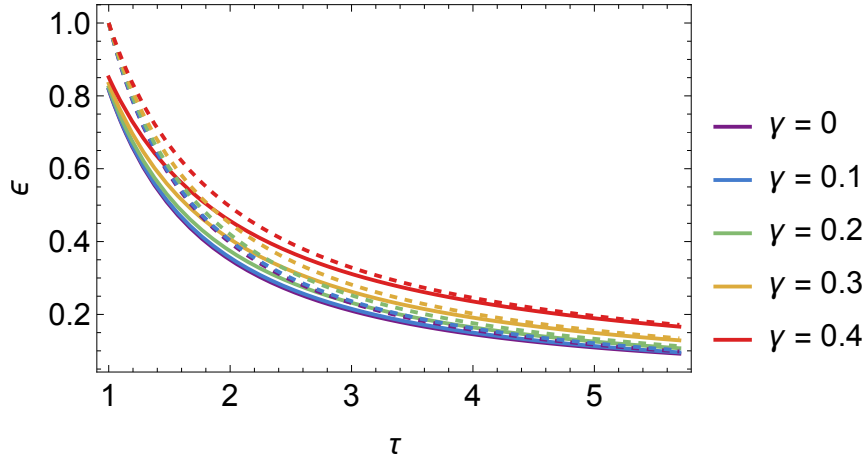


FIGURE 4.3: Energy density assuming ideal fluid (dashed) vs 1st order hydro (solid). We set $s_0 = T_0 = 1$.

4.5.1 Full solution

Remarkably, we can solve the equation (4.21) exactly. The **full solution** for the energy density with 1st hydro corrections is:

$$\epsilon(\tau) = \left(c_3 \tau^{2\gamma^2 - \frac{1}{3}} - \frac{c_4}{\tau} \right)^{\frac{3}{1-6\gamma^2} + 1} \quad (4.22)$$

where c_3 is an integration constant and:

$$c_4 = \frac{3^{\frac{3}{6\gamma^2-4}} (4 - 6\gamma^2)^{\frac{3}{4-6\gamma^2}} (6\gamma^2 - 1) \Sigma_0}{4\pi (3\gamma^2 - 2)}$$

Again, we can see how **the viscosity is described by the coefficient c_4** , which is suppressed by τ^{-1} in the late time limit whereas c_3 is suppressed by a factor $2\gamma^2 - \frac{1}{3}$ which for our range of γ 's is $(-\frac{1}{3}, 0)$. Let's analyze the full hydro solution (4.22) with some plots. In order to visualize the solution and since it depends on s_0 and T_0 , whose values are not obvious, we are going to set them to 1 for plotting purposes. Note that this is a qualitative analysis, even though the real behaviour is equivalent, just shifted in time. The results can be seen in Figures 4.3 and 4.4. It seems that the **larger γ is, the quicker it is described by an ideal fluid.**

Late time expansion

Let's try now study analytically the full hydro solution (4.22) by expanding some terms. Firstly, we rewrite the solution as:

$$\epsilon(\tau) = \left(-\frac{a}{\tau} + c_3 \tau^b \right)^c$$

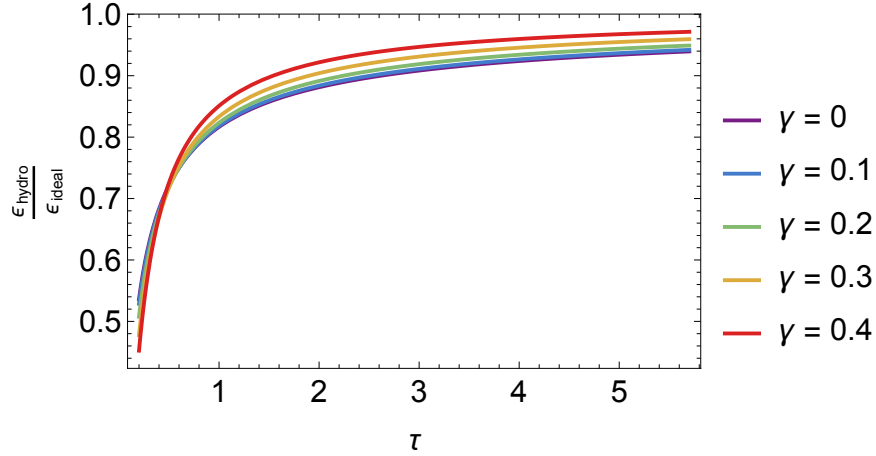


FIGURE 4.4: Energy density assuming ideal fluid (dashed) over energy density assuming 1st order hydro (solid). We set $s_0 = T_0 = 1$.

where c_3 is the same integration constant as before and now the new coefficients are:

$$a = \frac{3^{\frac{3}{6\gamma^2-4}} (4 - 6\gamma^2)^{\frac{3}{4-6\gamma^2}} (6\gamma^2 - 1) \Sigma_0}{4\pi (3\gamma^2 - 2)}$$

$$b = 2\gamma^2 - \frac{1}{3}$$

$$c = \frac{3}{1 - 6\gamma^2} + 1$$

Since $0 < a < \frac{s_0}{2\sqrt{2} \cdot 3^{3/4} \pi (s_0 T_0)^{3/4}}$, $-\frac{1}{3} < b < 0$, and $c > 4$ for our range of γ 's, we can expand this in a Taylor series for $\tau \rightarrow \infty$. The dominant term at late times is the ideal one, $c_3 \tau^{-(1/3)+2\gamma^2}$. We can rewrite $(-\frac{a}{\tau} + \tau^b c_3)^c$ as $(\tau^b c_3)^c \left(1 - \frac{a}{\tau^{b+1} c_3}\right)^c$ and expand the second term up to second order since we assume that $\frac{a}{\tau^{b+1} c_3} \ll 1$ at late times. Therefore, we find that in the late time limit the energy behaves as:

$$\epsilon(\tau) = \frac{D_\gamma}{\tau^{\frac{4}{3}-2\gamma^2}} - \frac{E_\gamma}{\tau^2} - \frac{F_\gamma}{\tau^{2\gamma^2+\frac{8}{3}}} \quad (4.23)$$

where the coefficients are:

$$D_\gamma = c_3^{\frac{3}{1-6\gamma^2}+1}$$

$$E_\gamma = \frac{27^{\frac{1}{6\gamma^2-4}} (4 - 6\gamma^2)^{\frac{3}{4-6\gamma^2}} \Sigma_0 c_3^{\frac{3}{1-6\gamma^2}}}{2\pi}$$

$$F_\gamma = \frac{3^{\frac{3}{3\gamma^2-2}+1} (4 - 6\gamma^2)^{\frac{3}{2-3\gamma^2}} \Sigma_0^2 c_1^{\frac{3}{1-6\gamma^2}-1}}{16\pi^2 (3\gamma^2 - 2)}$$

Hence, we have found **the generalization of the late time Bjorken flow for non conformal plasmas with 1st order hydro**. It is clear from (4.23) that the viscous corrections are described by the coefficients E_γ and F_γ . Since the coefficients are regular in our range of γ 's, we can claim that, **at late times, the viscous correction remain small, suggesting that the system does not fall out of equilibrium**.

However, this argument is not definitive, as (4.22) neglects corrections to $p/\epsilon = -2\gamma^2 + 1/3$ at low energies. We will later suggest a more robust argument that could support the claim that our system remains in equilibrium, based on quasinormal modes of the static black brane solutions.

Before that, let us present the full numerical dynamic evolution of the system and reveal the unbounded growth of curvatures in the bulk, which is the main goal of this thesis.

Chapter 5

Full microscopic evolution

In this chapter, we aim to compute dynamic boost-invariant solutions to the action described in (3.1), with a boundary conformal to a four-dimensional flat metric. This approach allows us to investigate the out-of-equilibrium behaviour of a strongly-coupled fluid in the central rapidity region produced in a heavy ion collision. For the numerical implementation, we follow the same approach as in [57, 6].

5.1 Dynamic solutions

5.1.1 Characteristic formulation of General Relativity

Solving Einstein's equations numerically can pose significant challenges. For instance, the full simulation of a binary black hole merger only became attainable in 2005 [55]. However, within the realm of gauge/gravity duality, a more tractable computational strategy emerges. This method, known as the 'characteristic' formulation, finds its origins in the pioneering work of Bondi [13, 14] and Sachs [56] during the 1960s, as they delved into the behavior of gravitational waves in flat space. Subsequently, Chesler and Yaffe [21, 22] conveniently adapted and applied this formulation to the AdS spacetime. The primary simplification involves transforming the coupled partial differential equations into a nested set of linear ordinary differential equations (ODEs). To accomplish this, three crucial steps must be taken:

- Partially fix diffeomorphism invariance through the utilization of generalized ingoing Eddington-Finkelstein coordinates. In this way, trajectories characterized by varying the radial coordinate r (while keeping the other coordinates constant) are, in fact, null geodesics.
- The spatial part of the metric's determinant must be a single function.
- One should employ derivatives along outgoing null rays instead of expressing Einstein's equations directly in terms of time derivatives.

5.1.2 The bulk metric ansatz

We are interested in full dynamical solutions to 3.1 that are asymptotically AdS_5 . A convenient metric ansatz written in Fefferman-Graham coordinates is:

$$ds^2 = \frac{L^2}{z^2} (-f(z, \tau) dt^2 + g(z, \tau) d\vec{x}^2 + dz^2).$$

Nevertheless, it is more convenient for the numerical implementation, as we have explained in the previous subsection, to write our ansatz for the $5d$ metric in generalized infalling Eddington Finkelstein coordinates as in [20]:

$$ds^2 = -Ad\tau^2 + S^2(e^{-2B}dy^2 + e^B dx_1^2 + e^B dx_2^2) + 2drd\tau \quad (5.1)$$

where we allow anisotropy between the longitudinal direction x_{\parallel} and the transverse plane $\vec{x}_{\perp} = (x_1, x_2)$. The metric functions depend only on proper time τ and the bulk radial holographic coordinate r , i.e. $A = A(r, \tau)$, $B = B(r, \tau)$ and $S = S(r, \tau)$, since we are considering a boost invariant case and we assume rotational symmetry in the transversal plane. The heavy ions will collide along z , and \mathbf{x}_{\perp} represents the two orthogonal directions $x_{\perp} = x_1, x_2$. It should be noted that τ serves as a null temporal coordinate (typically denoted as v in EF coordinates), meaning that surfaces of constant τ are not spacelike but null.

5.1.3 Gauge Freedom

It is important to recognize that the metric ansatz (5.1), as we have constructed it, remains invariant under the following set of transformations:

$$\begin{aligned} r &\rightarrow \tilde{r} = r + \xi(\tau) \\ S &\rightarrow \tilde{S} = S \\ B &\rightarrow \tilde{B} = B \\ A &\rightarrow \tilde{A} = A + 2\partial_{\tau}\xi(\tau) \end{aligned} \quad (5.2)$$

5.1.4 Nested structure

Using the so called Bondi-Sachs formulation [21], the equations of motion (3.2) are decoupled in a nested structure, allowing us to solve them without taking any approximation. In order to do so, we define the dotted derivative as a time derivative along a null geodesic and the prime derivative as the radial derivative along the holographic direction r :

$$\begin{aligned} \dot{h} &\equiv \partial_{\tau}h + \frac{1}{2}A\partial_r h \\ h' &\equiv \partial_r h \end{aligned}$$

and write the equations of motion for our metric ansatz (5.1) in terms of them as

$$\begin{aligned} S'' &= -\frac{1}{6}S \left(3(B')^2 + 4(\phi')^2 \right) \\ S\dot{S}' &= -\frac{2}{3}(S^2V(\phi) + 3\dot{S}S') \\ 2S\dot{B}' &= -3(\dot{S}B' + \dot{B}S') \\ 2S\dot{\phi}' &= SV'(\phi) - 3(\dot{\phi}S' + \dot{S}\phi') \\ S^2A'' &= S^2 \left(-3\dot{B}B' + \frac{4V(\phi)}{3} - 4\dot{\phi}\phi' \right) + 12\dot{S}S' \\ \dot{S} &= \frac{1}{6}(3\dot{S}A' - S(3\dot{B}^2 + 4\dot{\phi}^2)). \end{aligned} \quad (5.3)$$

Remarkably and as we have anticipated, the complicated PDE's have drastically simplified into a nested set of linear ODE's. In general, solving second-order differential equations requires boundary conditions. To address this, we impose specific values for the metric functions and their first derivatives at the boundary, ensuring that the boundary metric is conformally flat. This approach allows us to accurately determine the behavior of the solution near the boundary.

5.1.5 Near boundary expansion

In order to impose boundary condition for the EFE and make connection with the dual theory, we are interested in solving the equations of motion near the boundary. Notice that we want our bulk theory to be asymptotically AdS₅ so let us study how the metric should behave in that region. The AdS₅ spacetime metric in five dimensions can be written in Poincaré as:

$$ds_{\text{AdS}_5}^2 = \left(\frac{r}{L}\right)^2 (-dt^2 + dx^2 + dy^2 + dz^2) + L^2 \frac{dr^2}{r^2} \quad (5.4)$$

Therefore, the metric in the boundary where $r \rightarrow \infty$ and $dr = 0$ reads:

$$ds_{\partial\text{AdS}_5}^2 = \left(\frac{r}{L}\right)^2 (-dt^2 + dx^2 + dy^2 + dz^2). \quad (5.5)$$

Notice that is conformally flat with a conformal factor of r^2/L^2 . The ansatz for the bulk metric of our theory (5.1) near the boundary reads:

$$ds_B^2 = -Ad\tau^2 + S^2(e^{-2B}dy^2 + e^B dx_1^2 + e^B dx_2^2). \quad (5.6)$$

Comparing the metric (5.6) with the boundary metric of AdS₅ (5.5) and setting $L = 1$, it is clear that the metric functions should scale near the boundary with r as

$$A \sim r^2 \quad S \sim r \quad B \sim 1$$

and for the scalar field, the equations of motion near the boundary impose that it should scale as

$$\phi \sim \frac{\phi_0}{r^{d-\Delta}} + \frac{\phi_2}{r^\Delta} = \frac{\phi_0}{r} + \frac{\phi_2}{r^3}$$

where r is the radial holographic coordinate and for our theory $\Delta = 3$ and $d = 4$. Therefore we can be expand the metric functions and the scalar field near the boundary as:

$$A(r, \tau) = \sum_{n=0}^{\infty} a_n(\tau) r^{2-n} \quad (5.7)$$

$$S(r, \tau) = \sum_{n=0}^{\infty} s_n(\tau) r^{1-n} \quad (5.8)$$

$$B(r, \tau) = \sum_{n=0}^{\infty} b_n(\tau) r^{-n} \quad (5.9)$$

$$\phi(r, \tau) = \sum_{n=0}^{\infty} \phi_n(\tau) r^{-n-1} \quad (5.10)$$

where the time dependence is now only in the coefficients. In order to solve for the coefficients, we impose the ansatz metric near the boundary to be conformally equal to the flat metric in Milner coordinates (4.3). This fixes the following coefficients:

$$a_0 = 1 \quad , \quad s_0(t) = \sqrt[3]{\tau} \quad \text{and} \quad b_0(t) = -\frac{2}{3} \log(\tau)$$

Then, we expand the fields near the boundary and solve the equations of motion order by order plugging in the potential from our model (3.1) and the result is

$$A(r, \tau) = r^2 + 2\bar{\zeta}(\tau)r + \left(-\frac{2}{3}\Lambda^2 + \bar{\zeta}(\tau)^2 - 2\bar{\zeta}'(\tau) \right) + \frac{a_4(\tau)}{r^2} + \mathcal{O}\left(\frac{1}{r^3}\right) \quad (5.11)$$

$$S(r, \tau) = \sqrt[3]{\tau}r + \frac{1 + 3\tau\bar{\zeta}(\tau)}{3\tau^{2/3}} + \frac{-1 - 3\Lambda^2\tau^2}{9\tau^{5/3}r} + \mathcal{O}\left(\frac{1}{r^2}\right) \quad (5.12)$$

$$B(r, \tau) = -\frac{2\log(\tau)}{3} - \frac{2}{3\tau r} + \frac{1 + 2\tau\bar{\zeta}(\tau)}{3\tau^2 r^2} + \mathcal{O}\left(\frac{1}{r^3}\right) \quad (5.13)$$

$$\phi(r, \tau) = \frac{\Lambda}{r} - \Lambda \frac{\bar{\zeta}(\tau)}{r^2} + \frac{\phi_2(\tau)}{r^3} + \mathcal{O}\left(\frac{1}{r^4}\right). \quad (5.14)$$

Here, we display only the leading order terms and the initial appearance of the coefficients that are not determined by the asymptotic expansion of the equations, i.e. $a_1(\tau)$, $a_4(\tau)$, $b_4(\tau)$, ϕ_0 and $\phi_2(\tau)$. The constant ϕ_0 represents the source of the operator dual to ϕ , establishing the energy scale $\phi_0 \equiv \Lambda$ for the explicit breaking of conformal symmetry in the UV. In fact, we use this scale to set the units for various quantities that we display later in this thesis.

Additionally, $\bar{\zeta}(\tau)$ represents a residual gauge freedom that we use to fix the location of the apparent horizon. Indeed, $a_1(\tau) = 2\bar{\zeta}(\tau)$ encodes the residual gauge freedom in the metric $r \rightarrow r + \bar{\zeta}(\tau)$. We can explicitly see this by performing the gauge transformation in the metric (5.1) and realizing that $A(r, \tau)$ has to transform as:

$$A \rightarrow A + 2\partial_\tau \bar{\zeta}$$

in order to be invariant as we previously mentioned. This fixes $a_1(\tau) = 2\bar{\zeta}(\tau)$ in the near boundary expansion and we use this residual gauge freedom to fix the position of the apparent horizon. In solving order by order, we discover that $a_4(\tau)$ is not determined but its time derivative is. Hence, we take it as a constraint which has to be obeyed at every time step:

$$\begin{aligned} \partial_\tau a_4 = \frac{4}{81\tau^5} & \left(-27a_4\tau^4 - 54b_4\tau^4 + j_1\tau^2 (2j_1 (27\bar{\zeta}\tau^3\bar{\zeta}' + (3\bar{\zeta}\tau + 2)^2) \right. \\ & \left. + 4j_1^3\tau^2 - 9\tau^2 (3\tau\phi_2' + 2\phi_2) \right) + 9(2\bar{\zeta}\tau + 1)(2\bar{\zeta}\tau(\bar{\zeta}\tau + 1) + 1). \end{aligned} \quad (5.15)$$

Lastly, $a_4(\tau)$, $b_4(\tau)$, and $\phi_2(\tau)$ are associated with the evolution of the energy, pressure, and vacuum expectation value of the operator in our system. In fact, holography enables us to access the expectation value of the microscopic energy-momentum tensor [45, 11], as we will in the next section.

5.1.6 Gauge Fixing

We would like to keep our horizon fixed in the bulk radial coordinate r since our numerical grid is finite and the horizon could easily exit it, which would not be

desirable. Therefore, we want to constraint the remaining gauge freedom (5.2). An effective way to do it involves treating $\zeta(\tau)$ as an additional evolving parameter and determining its evolution equation by imposing the apparent horizon to remain fixed at a constant radial position $r = r_h$. Hence, we aim to enforce the conditions

$$\Theta|_{r=r_h} = 0, \quad \partial_\tau \Theta|_{r=r_h} = 0 \quad (5.16)$$

consistently throughout the evolution, where Θ represents the expansion of outgoing null geodesics for our metric (5.1). At surfaces with constant r , Θ is expressed as

$$\Theta = -3S^2\dot{S}. \quad (5.17)$$

To impose the conditions (5.16) numerically, a straightforward approach is given by

$$(\partial_\tau \dot{S} + \kappa \dot{S})|_{r=r_h} = 0, \quad (5.18)$$

where κ is a positive parameter typically set to 1. This approach offers the advantage of driving the $\dot{S} = 0$ surface back to $r = r_h$ whenever numerical inaccuracies accumulate, proving highly effective in practical applications. Expanding (5.18) and using the constraint equation yields an equation for $\partial_\tau \zeta$ to be evaluated at $r = r_h$. Solving for this equation at every time step allows us to numerically control the time evolution of $\zeta(\tau)$.

5.1.7 Field redefinitions

To solve the system of differential equations, it is advantageous to use $z = \frac{1}{r}$ as the radial holographic coordinate. The idea is to redefine the evolved fields to eliminate the divergent terms at the boundary where $z = 0$. For that purpose, we implicitly define the finite fields at the boundary as:

$$\begin{aligned} A(z, \tau) &\equiv z^2 A_f(z, \tau) - \frac{2\Lambda^2}{3} - 2\zeta'(\tau) + \zeta(\tau)^2 + \frac{2\zeta(\tau)}{z} + \frac{1}{z^2} \\ S(z, \tau) &\equiv z^2 S_f(z, \tau) + \frac{18\tau^2 \zeta(\tau) + \tau^2 \left(\frac{18}{z} - 6\Lambda^2 z\right) + 6\tau - 2z}{18\tau^{5/3}} \\ B(z, \tau) &\equiv z^4 B_f(z, \tau) - \frac{18\tau^3 \log(\tau) + 2\tau^2 z (2\Lambda^2 z^2 + 9) + 18\tau z^2 \zeta(\tau) (\tau z \zeta(\tau) - \tau + z) - 9\tau z^2 + 6z^3}{27\tau^3} \\ \phi(z, \tau) &\equiv z^3 \phi_f(z, \tau) - \frac{1}{2} \Lambda z (2z \zeta(\tau) - 2) \\ \dot{S}(z, \tau) &\equiv z^2 \dot{S}_f(z, \tau) + \frac{81\tau^3 - 3\Lambda^2 \tau^2 z^2 (9\tau + 4z) + 27\tau^2 z \zeta(\tau) (3\tau z \zeta(\tau) + 6\tau + 2z) + 54\tau^2 z - 27\tau z^2 + 20z^3}{162\tau^{8/3} z^2} \\ \dot{B}(z, \tau) &\equiv z^3 \dot{B}_f(z, \tau) - \frac{\tau^2 + \tau z^2 \zeta(\tau) - \tau z + z^2}{3\tau^3} \\ \dot{\phi}(z, \tau) &\equiv z^2 \dot{\phi}_f(z, \tau) - \frac{\Lambda}{2}. \end{aligned}$$

5.1.8 Evolution Algorithm

We now have everything we need to solve the equations of motion in nested form. We employ the following iterative procedure. Note that the same strategy holds even without the presence of a scalar field. At each given time step τ_n , we solve the radial ordinary differential equations (ODEs) at every null time slice as follows:

- We start at a given time τ_n with the first radial ODE for $S(r, \tau_n)$ by providing an initial radial profile for $B(r, \tau_n)$ and $\phi(r, \tau_n)$ and the value of $a_4(\tau_n)$ and $\xi(\tau_n)$. Once these quantities are known, we solve for $S(r, \tau_n)$.
- Next, we move to the second radial ODE and solve for $\dot{S}(r, \tau_n)$, given that $S(r, \tau_n)$ is already known.
- We proceed to solve the remaining equations successively in the same manner. Note that the last equation is redundant and serves as a constraint. We can numerically track this constraint to assess the accuracy of our solution and estimate the numerical error.
- With all the metric functions determined, we compute $\partial_\tau \xi(\tau_n)$ using (5.18). Then, we calculate $\partial_\tau B(r, \tau_n)$ and $\partial_\tau \phi(r, \tau_n)$ from the definitions of the dotted derivatives of the obtained $\dot{B}(r, \tau_n)$ and $\dot{\phi}(r, \tau_n)$. Finally, we obtain $\partial_\tau a_4(\tau_n)$ using (5.15).
- We then advance $\xi(\tau_n)$, $B(r, \tau_n)$, $\phi(r, \tau_n)$ and $a_4(\tau_n)$ to the next time step τ_{n+1} using a time integrator method such as Adams–Bashforth, Runge–Kutta, Euler method or similar.
- Finally, we return to the first step and repeat the process at time τ_{n+1} .

5.1.9 Discretization and spectral methods

The equations of motion (5.3) are integrated over the holographic coordinate z at every time step. To discretize the equations in this direction, we use a set of points called a partition. In our case, this partition, denoted as z , consists of $N + 1$ Chebyshev–Gauss–Lobatto (CGL) points:

$$z_i = \cos\left(\frac{\pi i}{N}\right) \quad (i = 0, 1, \dots, N).$$

These points are placed in the range $z \in [0, 1]$. Note that the range limits correspond to the boundary ($z = 0$) and the black hole apparent horizon, typically set at ($z = 1$). Since it is at these points where we read the physics of our system, it is desirable to have a higher density of grid points there, and the CGL points fulfill this requirement. The primary operation in the z direction involves computing partial derivatives as given in equations (5.3). To compute these derivatives, we employ pseudo-spectral¹ methods [15]. This approach involves expressing the solution of the differential equations as a series of specific basis functions, which in our case are Chebyshev polynomials T_n , essentially cosine functions in disguise. The coefficients of these basis functions are then determined to approximate the solution of the differential equation as accurately as possible. To compute derivatives, we use the Chebyshev differentiation matrix D_N , which is defined element-wise for $N \geq 1$

¹While both spectral and pseudo-spectral methods aim to approximate solutions with high accuracy, spectral methods do so by expanding the solution in terms of global basis functions and projecting the equations onto these functions, whereas pseudo-spectral methods enforce the differential equation at discrete collocation points and approximate derivatives using differentiation matrices.

points by:

$$\begin{aligned} (D_N)_{00} &= \frac{2N^2 + 1}{6}, & (D_N)_{NN} &= -\frac{2N^2 + 1}{6}, \\ (D_N)_{jj} &= -\frac{x_j}{2(1 - x_j^2)}, & j &= 1, \dots, N - 1, \\ (D_N)_{ij} &= \frac{c_i(-1)^{i+j}}{c_j(x_i - x_j)}, & i &\neq j, \quad i, j = 0, \dots, N, \end{aligned}$$

where

$$c_i = \begin{cases} 2 & \text{if } i = 0, N \\ 1 & \text{otherwise.} \end{cases}$$

Higher-order differentiation matrices can be easily obtained by multiplying the differentiation matrix D_N by itself: $D_N^{(m)} = D_N^m$.

5.2 Thermodynamics

We want to compute the thermodynamics quantities and the expectation values from dynamical variables in terms of the bulk metric ansatz (5.1) and its boundary information. We are going to follow the prescription explained in section 3.3. Throughout this section we use $c = \hbar = k_B = 1$.

5.2.1 Bekenstein-Hawking entropy

Given our ansatz for the bulk metric (5.1) the induced metric on the black brane horizon can be derived setting $d\tau = dr = 0$:

$$d\ell^2 = g_{ij}x^i x^j = \Sigma^2 \left(e^{-2B} dy^2 + e^B d\bar{x}_\perp^2 \right).$$

The determinant of the induced metric tensor g_{ij} for these coordinates $(y, x_\perp^1, x_\perp^2)$ is then:

$$\det(g_{ij}) = \Sigma^6$$

which allows us to compute the area element dA :

$$dA = \sqrt{\det(g_{ij})} dy dx_\perp^1 dx_\perp^2 = \Sigma^3 dy dx_\perp^1 dx_\perp^2.$$

To find the total area, we should integrate this area element over the ranges of y, x_\perp^1 , and x_\perp^2 :

$$\text{Area} = \int \Sigma^3 dy dx_\perp^1 dx_\perp^2.$$

Unfortunately, these coordinates are unbounded and the area diverges. In other words, we are not able to compute the total entropy because the total "area" of the horizon is infinite. Instead, we can actually compute the entropy density since we know the "area" density:

$$s = \frac{a_H}{4G_N} = \frac{\Sigma^3(z_H)}{4G_N} = \frac{2}{\kappa_5^2} \pi \Sigma^3(z_H)$$

where $s = \frac{dS}{dydx_{\perp}^1 dx_{\perp}^2}$ is the entropy density and $a_H = \frac{dA}{dydx_{\perp}^1 dx_{\perp}^2}$ is the "area" density of the horizon.

5.2.2 Hawking Temperature

Computing the temperature of a black hole using the method of imposing regularity in Euclidean space is more subtle in our metric ansatz since we have a non-diagonal term in $d\tau dr$ that comes from expressing our bulk metric ansatz (5.1) in Eddington Finkelstein coordinates. In order to remove the cross term that would become complex after the Wick rotation, we undo the Eddington Finkelstein change of coordinates:

$$\begin{aligned}\tau &= t + r^* \\ \frac{dr^*}{dr} &= \frac{1}{A}\end{aligned}$$

Thus, in the original (t, r) coordinates the metric ansatz becomes:

$$ds^2 = -A dt^2 + \frac{1}{A} dr^2 + \Sigma^2 \left(e^{-2B} dy^2 + e^B d\vec{x}_{\perp}^2 \right) \quad (5.19)$$

where $A(r, t)$ is assumed to have a first-order zero at the horizon $r = r_H$, while $\Sigma(r, t)$ remains non-zero there. For notational simplicity we are going to ignore the time dependence throughout this subsection. Following the conventional approach [33], we perform a Wick rotation $t \rightarrow -it_E$ in order to get the Euclidean analytical continuation of the metric

$$ds_E^2 = A dt_E^2 + \frac{1}{A} dr^2 + \Sigma^2 \left(e^{-2B} dy^2 + e^B d\vec{x}_{\perp}^2 \right). \quad (5.20)$$

Since we want to impose regularity at the horizon, we can expand our metric near the horizon $r \simeq r_H$:

$$ds_E^2 = A'(r_H)(r - r_H) dt_E^2 + \frac{1}{A'(r_H)(r - r_H)} dr^2 + \Sigma^2 \left(e^{-2B} dy^2 + e^B d\vec{x}_{\perp}^2 \right). \quad (5.21)$$

Introducing radial and angular coordinates:

$$\rho = 2\sqrt{\frac{r - r_H}{A'(r_H)}}, \quad \theta = \frac{t_E}{2} A'(r_H) \quad (5.22)$$

allows us to write the metric as

$$ds_E^2 \simeq d\rho^2 + \rho^2 d\theta^2 + g(r_H) d\vec{x}_{\perp}^2. \quad (5.23)$$

Notice that in these new coordinates the first two terms of the metric represent a plane in polar coordinates. Therefore, in order to avoid a conical singularity at $\rho = 0$ we must demand θ to have a periodicity of 2π . Moreover, from statistical field theory we know that Euclidean time is periodic with a periodicity of $\beta = \frac{1}{T}$. By equating both periods, we are left with an expression for the temperature of the black brane:

$$\boxed{T = \frac{A'(r_H)}{4\pi} \xrightarrow{z=1/r} \frac{-z_H^2 A'(z_H)}{4\pi}} \quad (5.24)$$

It is important to note that the Euclidean metric is not describing the spacetime inside the horizon $r < r_H$ since the origin of the polar coordinates is in the horizon itself. In fact, Hawking original formula for the temperature is written in terms of κ , which is the surface gravity at the horizon:

$$T = \frac{\kappa}{2\pi}$$

from which we can identify the surface gravity at the horizon for our metric ansatz:

$$\kappa = \frac{A'(r_H)}{2} \xrightarrow{z=1/r} \frac{-z_H^2 A'(z_H)}{2}$$

5.2.3 Holographic renormalization

In order to compute the energy momentum tensor of the dual field theory is more convenient to express our metric in Fefferman-Graham coordinates

$$ds^2 = \frac{L^2}{z^2} (dz^2 + g_{\mu\nu} dx^\mu dx^\nu)$$

Therefore we can apply the result from [45]. Then, we expand the metric and the scalar field in terms of the holographic coordinate z , in the limit where $z \rightarrow 0$. The asymptotic expansion for the metric in EF coordinates and the scalar field read:

$$ds^2 = z^2 \left(g_{\mu\nu}^{(0)}(t) + g_{\mu\nu}^{(2)}(t)z^2 + g_{\mu\nu}^{(4)}(t)z^4 + \dots \right), \quad (5.25)$$

$$\phi = \Lambda z + \phi_v(t)z^3 + \dots \quad (5.26)$$

where $t \equiv t_{FG}$. Therefore, the expectation values of the field theory operators can be expressed as follows:

$$\langle T_{\mu\nu} \rangle = \frac{2L^3}{\kappa_5^2} \left(g_{\mu\nu}^{(4)}(t) + \left(\Lambda \phi_v(t) - \frac{\Lambda^4}{18} - \frac{\gamma^2 \Lambda^4}{6} \right) \eta_{\mu\nu}(t) \right), \quad (5.27)$$

$$\langle O \rangle = -\frac{2L^3}{\kappa_5^2} \left(2\phi_v(t) + \frac{2\gamma^2 \Lambda^3}{3} \right) \quad (5.28)$$

where $g_{\mu\nu}^{(0)}(t_{FG}) = \eta_{\mu\nu}(t_{FG})$. As anticipated, equations (5.27) and (5.28) lead to the Ward identity for the trace of the stress tensor:

$$T_\mu^\mu = -\Lambda \langle O \rangle, \quad (5.29)$$

and we adopt a renormalization scheme where $\langle T_\mu^\nu \rangle = \langle O \rangle = 0$ in the vacuum. Therefore, we will omit the expectation value notation and work with rescaled quantities:

$$\langle T_\nu^\mu \rangle = \frac{2L^3}{\kappa_5^2} \text{diag}(-\epsilon, p_\parallel, p_\perp, p_\perp). \quad (5.30)$$

Thus, we can write the thermodynamic quantities as a function of the boundary data in EF coordinates. Therefore, we can express the gauge theory values in terms of our

evolution variables (b_4, a_4, ϕ_v) as follows:

$$\begin{aligned}\epsilon(\tau) &= -\frac{3}{4}a_4(\tau) + \frac{1}{36}(6\gamma^2 + 7)\Lambda^4 + \Lambda^2\zeta(\tau)^2 - \Lambda\phi_v(\tau), \\ p_{\parallel}(\tau) &= \frac{1}{108\tau^4} \left\{ \tau \left[-\tau^3 \left(27a_4(\tau) + 216b_4(\tau) + (18\gamma^2 + 5)\Lambda^4 - 36\Lambda\phi_v(\tau) \right) \right. \right. \\ &\quad \left. \left. - 36\zeta(\tau)^2\tau(\Lambda^2\tau^2 - 6) + 48\zeta(\tau)(2\Lambda^2\tau^2 + 3) + 32\Lambda^2\tau + 144\zeta(\tau)^3\tau^2 \right] + 36 \right\}, \\ p_{\perp}(\tau) &= -\frac{1}{108\tau^4} \left\{ \tau \left[\tau^3 \left(27a_4(\tau) - 108b_4(\tau) + (18\gamma^2 + 5)\Lambda^4 - 36\Lambda\phi_v(\tau) \right) \right. \right. \\ &\quad \left. \left. + 36\zeta(\tau)^2\tau(\Lambda^2\tau^2 + 3) + 24\zeta(\tau)(2\Lambda^2\tau^2 + 3) + 16\Lambda^2\tau + 72\zeta(\tau)^3\tau^2 \right] + 18 \right\}.\end{aligned}$$

where p_{\perp} and p_{\parallel} are the transverse and longitudinal pressures. As we have pointed out, our system models the microscopic evolution of a strongly-coupled fluid akin to the quark-gluon plasma produced in heavy-ion collisions. After the formation of the quark-gluon plasma, the system undergoes expansion and cooling. The evolution of the energy density as a function of proper time can be seen in Figure 5.1. As we

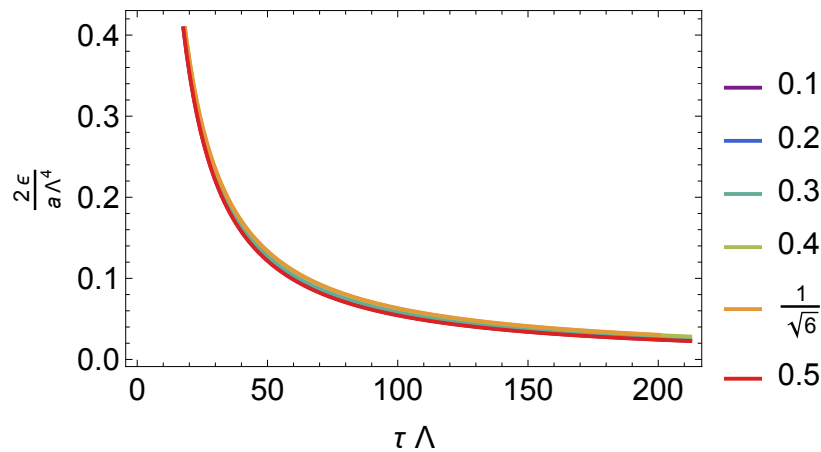


FIGURE 5.1: Energy density as a function of proper time.

may have expected, $\epsilon(\tau)$ decreases monotonically because the expansion dilutes the fluid, showing no significant dependence on γ . A natural question arises: does the hydrodynamic description adequately capture this process? To address this question, we display the ratio of pressures over the energy density and compare it to the hydrodynamic result from (4.7) for the particular case of $\gamma = 4/10$.

In particular, using the equation of state $p(\epsilon)$ and the energy dependence of the viscosities $\zeta(\epsilon)$ and $\eta(\epsilon)$ derived from the static black brane solutions, we can evaluate $p_{\parallel}(\epsilon(\tau))$ and $p_{\perp}(\epsilon(\tau))$. Comparing these to $p_{\parallel}(\tau)$ and $p_{\perp}(\tau)$, as shown in Figure 5.2, demonstrates a remarkable agreement, indicating that the system is well described by hydrodynamics shortly after the initial time.

In fact, the discrepancy between them rapidly diminishes to a relative value of approximately 10^{-5} , indicating the magnitude of higher-order terms in the gradient expansion of the hydrodynamic approximation as it can be seen in Figure 5.3. Once we verify that the hydrodynamic approximation accurately describes the evolution, we can ignore the bulk evolution and extend our results to later times (lower energies) by solving the hydrodynamic equation (4.9).

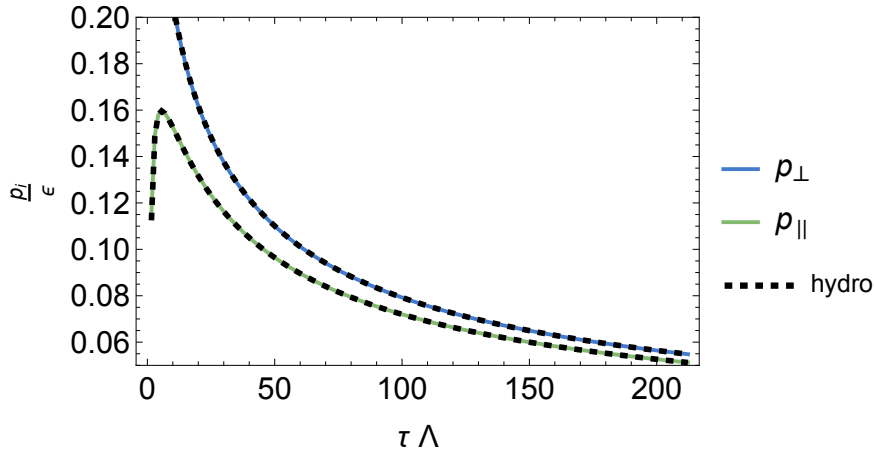


FIGURE 5.2: Comparison between the transverse and longitudinal pressures as obtained from the full microscopic evolution (solid lines) and their hydrodynamic approximation (dashed black), as a function of proper time.

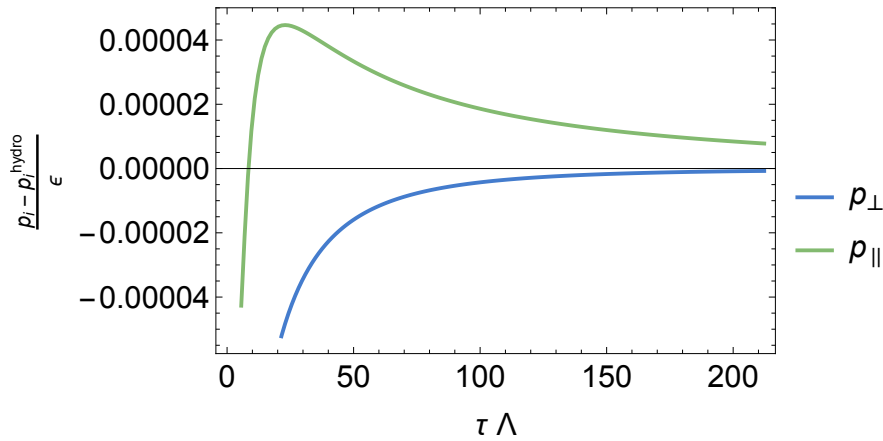


FIGURE 5.3: Difference between the full microscopic pressures and the hydrodynamic approximation, as a function of proper time.

By proceeding in this manner, our results hinge on the expectation that our system will not fall out of equilibrium again. Crucially, any perturbation in the fluid must relax faster than the fluid expands. While this is a natural expectation, it is not universally true. For instance, a fluid in an expanding de Sitter universe might fall out of equilibrium since the expansion rate is fixed by the cosmological constant, as discussed in Ref. [19]. In contrast, in our case, the expansion rate decays as $\epsilon'/\epsilon \simeq \tau^{-1}$.

The primary focus of this thesis is to investigate the growth of curvature invariants in the bulk. In the following chapter, we will explore this in detail and argue that our findings result from the hydrodynamization of the system, suggesting that our conclusions are broadly applicable.

Nevertheless, in the following section we evaluate the performance of our numerical code by showing several numerical checks. This is crucial, since all our results rely on this code.

5.3 Code performance

In this section we are going to assess the performance of the numerical code that we have used to solve the dynamic equations of motion by computing several numerical checks.

5.3.1 Apparent Horizon

The apparent horizon (AH) is a surface in spacetime that separates light rays moving towards a black hole from those moving away from it. It is defined as the boundary where the expansion of outgoing null geodesics becomes zero, indicated by $\dot{S} = 0$ as we have shown in (5.17). The AH typically surrounds a trapped surface, which is a (compact, orientable, space-like) surface with both inward and outward-pointing light-like normal vectors converging. The AH is the outermost trapped surface, known as the marginally outer trapped surface. Unlike the event horizon (EH), which is a global concept, the AH is a local concept and can be identified at a specific moment in time. It can change shape and position depending on the distribution of matter and energy nearby. In order to check the position of the AH, we want to plot several light rays and check that the AH behaves as it should. The light-like rays can be found by solving the geodesic equation for our metric ansatz [18]:

$$\frac{dr}{dt} = \frac{A(r, t)}{2} \xrightarrow{z=1/r} \frac{dz}{dt} = -z^2 \frac{A(z, t)}{2}.$$

In Figure 5.4, we show the evolution of the AH position in the (z, τ) plane. This

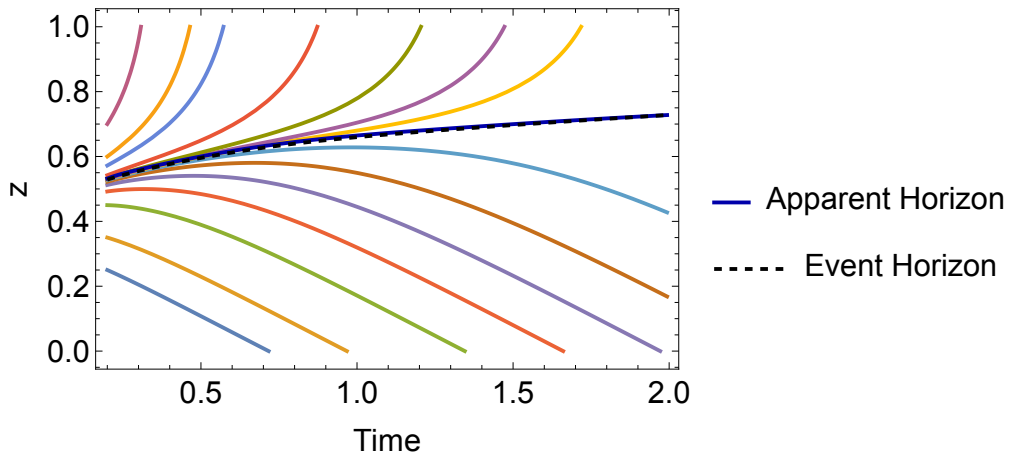


FIGURE 5.4: Time evolution of the apparent and event horizons in the (z, τ) plane. Light rays are also shown to illustrate whether they escape or fall into the horizon. The boundary is located at $z = 0$.

simulation was conducted in a boost-invariant setup without fixing the gauge $\xi(\tau)$, allowing the AH to move freely. The AH separates regions where light rays escape the horizon from those that fall into the black hole. As observed, the EH and AH coincide at equilibrium but generally differ out of equilibrium. Additionally, the slope of the light rays near the boundary is approximately $-1/2$, consistent with the geodesic equation evaluated near the boundary where $A(z, \tau) \simeq 1/z^2 + \mathcal{O}(1/z)$. Precisely because of the effect of the AH moving away from our grid, we fix the

gauge $\zeta(t)$ as explained in section 5.1.6. Fixing the AH is crucial for two main reasons. First, we do not want the AH to exit the grid, as several quantities are measured at the horizon. Second, by setting the AH at the limit of our grid, $z = 1$, we avoid simulating the interior of the black hole. This is important because the interior leads to numerical instabilities due to the proximity to singularities and is not relevant to our study, as the physics inside are causally disconnected from the exterior.

5.3.2 Convergence

The objective of this convergence check is to validate the numerical convergence of our simulations by varying the number of grid points N_z and consequently the time step $d\tau$, since they are related by $d\tau = \frac{1}{6N_z^2}$. We analyze observables including the constraint, energy density, and longitudinal and transverse pressures over time, ensuring they converge to consistent values as grid resolution increases. Grid points are taken at different positions in the holographic coordinate z : $N_z = 30, 40, 50, 60$.

The specific initial conditions chosen for this check are $z_H = \frac{999}{1000}$, $\gamma = \frac{1}{10}$, $\phi_2 = \frac{8}{10}$, $b_4 = 1$, $j_1 = 1$, $a_4 = -100$, and $\tau_i = \frac{2}{10}$.

In Figure 5.5, we show the results for the energy density, and the longitudinal and transverse pressures. Figure 5.6 presents the results for the constraint in a logarithmic plot, demonstrating the convergence of our system. This comparison validates that our results are robust across different grid resolutions.

We plot these observables against time, highlighting how they stabilize with increasing N_z , maintaining consistency with finer grid resolutions. The clear presentation and interpretation of these results underscore the reliability and accuracy of our numerical simulations.

In conclusion, the convergence analysis confirms that our simulation setup effectively captures the expected physical behavior as resolution improves, crucially impacting the reliability of our findings. As a final comment, we observe in Figure 5.6 that the constraint tends to grow. This typically poses a problem at late times, which we systematically address by increasing the number of grid points whenever the constraint becomes too high, ensuring the trustworthiness of the results.

5.3.3 Curvatures

In this numerical check, we aim to verify that the scalar curvatures we compute remain the same when changing the gauge, i.e., when altering the AH position. Since we evaluate the Ricci scalar, the squared Ricci scalar, and the Kretschmann scalar at the horizon r_H for every time step, we perform a gauge transformation on the holographic coordinate of the form $r \rightarrow r' = r + \zeta$, which shifts the horizon to $r_H \rightarrow r'_H = r_H + \zeta$.

If the code functions correctly, this gauge transformation should yield the same values for the curvature invariants evaluated at the new horizon. Since these are curvature invariants, they should not depend on the position of the horizon, which is merely a gauge choice. To test this, we have evaluated the curvatures for different gauges, i.e., for different choices of the event horizon radial position $z_H \in$

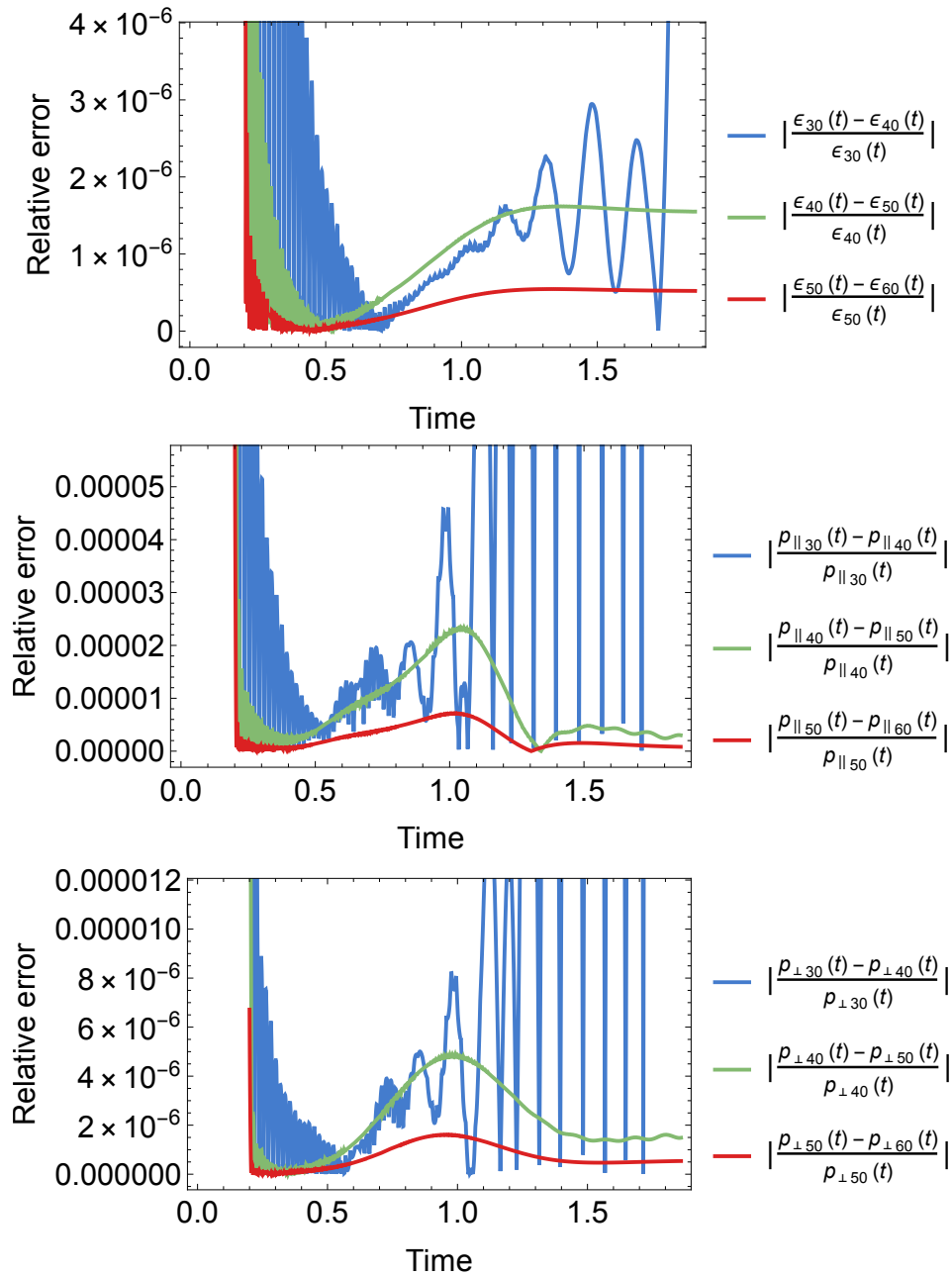


FIGURE 5.5: We show the absolute relative error of the energy density, as well as the longitudinal and transverse pressures, as a function of time for different numbers of grid points ($N = 30, 40, 50, 60$).

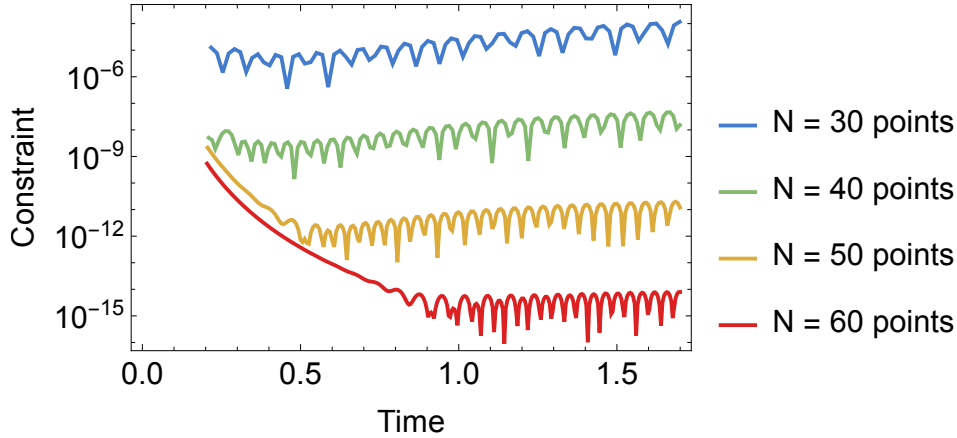


FIGURE 5.6: Logarithmic plot of the constraint as a function of time for different numbers of grid points ($N = 30, 40, 50, 60$).

[0.5, 0.6, 0.7, 0.8, 0.9, 0.999]. The results are shown in Figure 5.7. In Figure 5.8, we show how the relative error between the curvatures evaluated at different gauge choices decreases as we increase the number of grid points. We simulated using $N = 30, 40, 50, 60$ grid points and verified that the results converge as the number of points increases.

This gauge and convergence analysis confirms that our simulation accurately captures the expected physical behavior, demonstrating the reliability of our numerical methods.

5.3.4 Energy-Momentum Tensor Conservation

The conservation of the energy-momentum tensor provides us with a differential equation for the energy (4.9) that should hold at every time step. We rewrite it here for convenience:

$$\nabla_{\mu} T^{\mu\nu} = 0 \quad \rightarrow \quad \epsilon'(\tau) + \frac{\epsilon(\tau) + p_{\parallel}(\tau)}{\tau} = 0.$$

In Figure 5.9, we show the equation for the energy-momentum tensor conservation as a function of the number of grid points N , normalized by the energy density at every time step. We conclude that the energy-momentum conservation converges to zero as we increase the resolution of our grid, as expected.

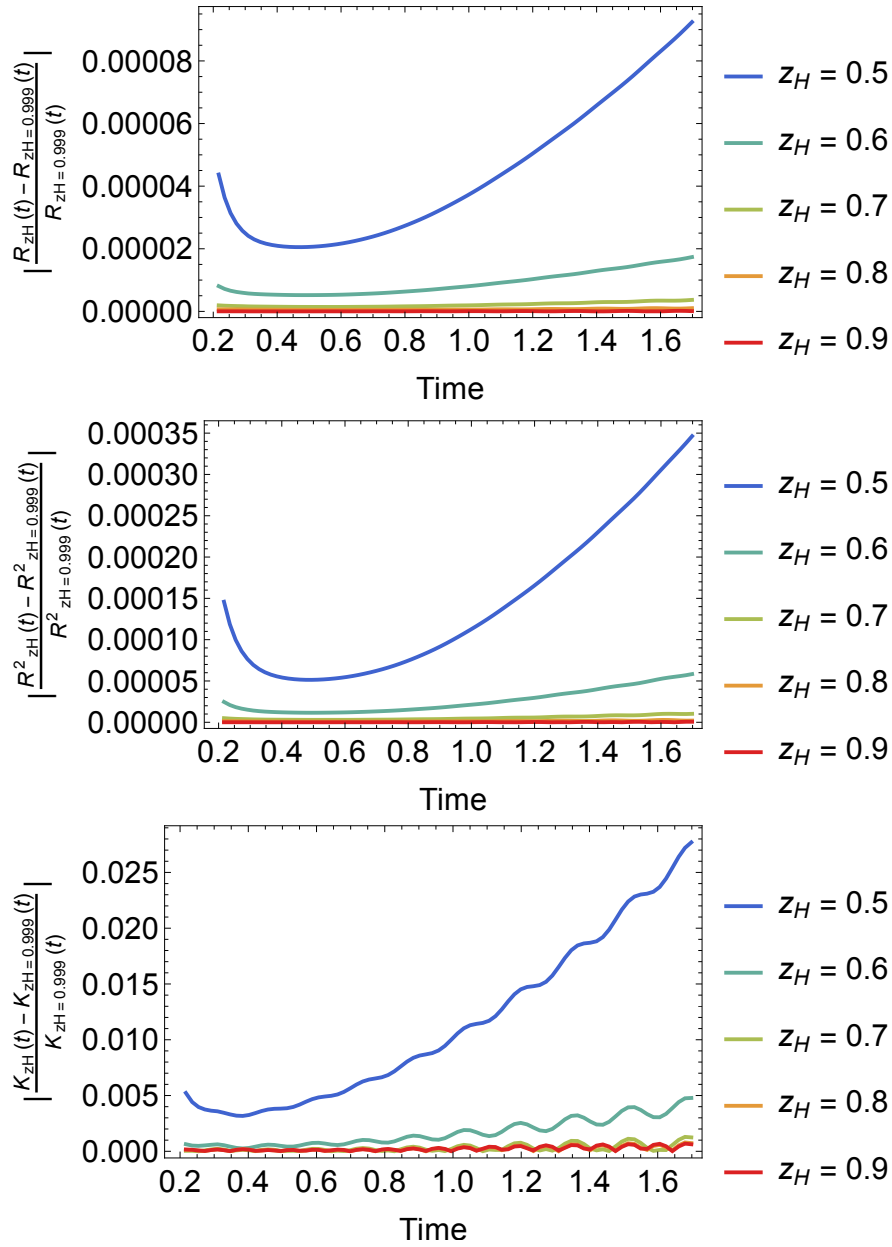


FIGURE 5.7: We compute the relative error between the scalar curvatures evaluated at different gauges, i.e. AH positions $z_H = 0.5, 0.6, 0.7, 0.8, 0.9$. We take as a reference the gauge with $z_H = \frac{999}{1000}$ for $N = 30$ grid points.

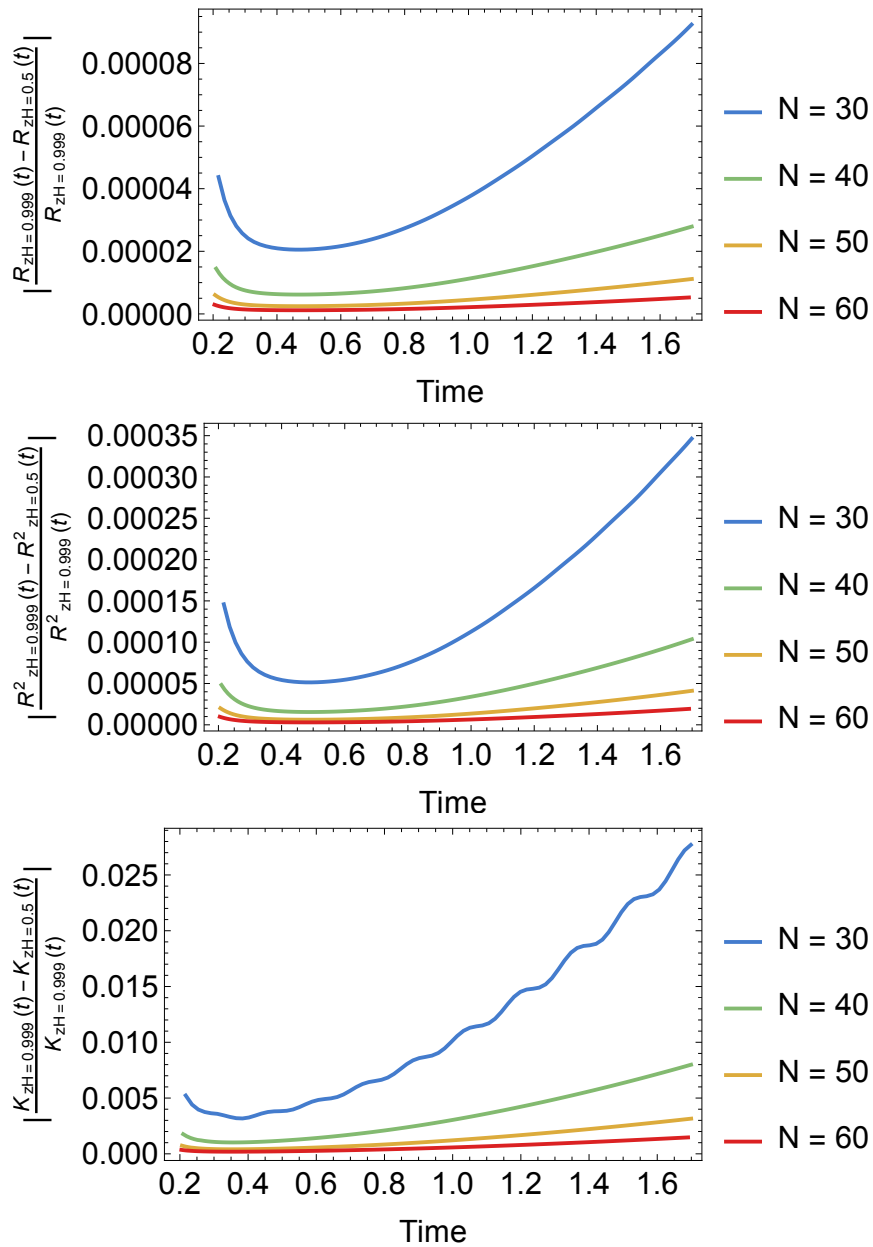


FIGURE 5.8: Absolute value of the relative error between the curvatures evaluated at the horizon for two different gauges $z_H = \frac{999}{1000}$ and $z_H = \frac{1}{2}$, as a function of the number of grid points ($N = 30, 40, 50, 60$).

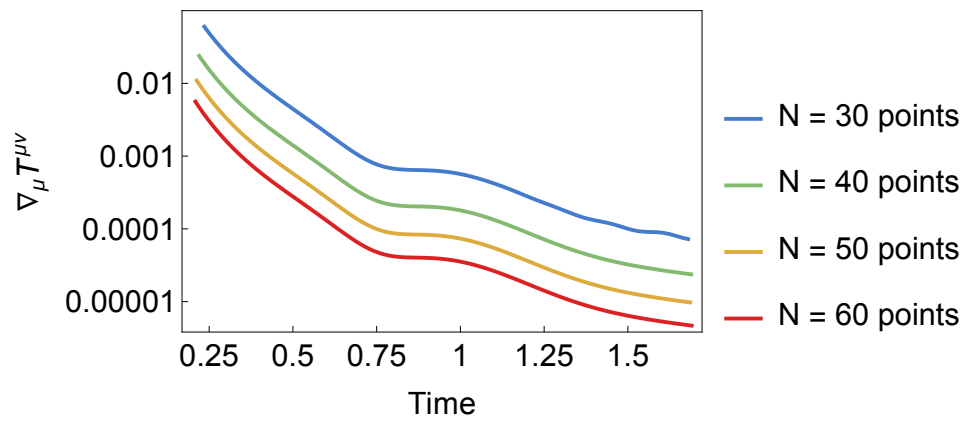


FIGURE 5.9: Energy-momentum tensor conservation normalized by the energy density as a function of time for different grid points ($N = 30, 40, 50, 60$).

Chapter 6

Cosmic Censorship

In this chapter, we aim to dynamically explore cosmic censorship by studying the value of curvature invariants at the black brane horizon. In fact, we expect the curvature invariants to grow at the horizon due to the existence of the unbounded exponential potential of our scalar field. We can directly see this from the Einstein field equations (EFE):

$$R_{\mu\nu} - \frac{1}{2}Rg_{\mu\nu} = 8\pi T_{\mu\nu}$$

where we set $G = 1$. After multiplying both sides by the inverse metric $g^{\mu\nu}$ and using the property that $g_{\mu\nu}g^{\mu\nu} = d$ where d is the spacetime dimension, the Ricci scalar is proportional to the trace of the energy momentum tensor:

$$R = -\frac{16}{3}\pi T_{\mu}^{\mu}.$$

On the other hand, we recall that the energy momentum tensor reads

$$T_{\mu\nu} = \frac{1}{8\pi} \left(2\partial_{\mu}\phi\partial_{\nu}\phi - g_{\mu\nu} \left[g^{\alpha\beta}\partial_{\alpha}\phi\partial_{\beta}\phi + 2V(\phi) \right] \right),$$

and taking the trace provides us with

$$T_{\mu}^{\mu} = -\frac{1}{8\pi} \left(3g^{\alpha\beta}\partial_{\alpha}\phi\partial_{\beta}\phi + 10V(\phi) \right)$$

so the Ricci scalar will be:

$$R = 2g^{\alpha\beta}\partial_{\alpha}\phi\partial_{\beta}\phi + \frac{20}{3}V(\phi). \quad (6.1)$$

It is clear from (6.1) that at late times, the Ricci scalar will grow since the scalar potential will be rolling down the unbounded potential while cooling down. In this sense, it is expected that the Ricci scalar evaluated at the horizon will tend to $-\infty$ as $\phi \rightarrow \infty$:

$$\lim_{\phi_H \rightarrow \infty} R_H \propto V(\phi_H) \rightarrow -\infty$$

which is exactly what happens in the numerical results that we will show later in the chapter. In particular, in the next section we will study the curvature invariants through the late time analytical solution of our model found by [44].

6.1 Analytical late time behaviour of curvature invariants

In order to study the late time behaviour of our non-conformal plasma as a function of proper time, we are going to follow the same approach as in [44], where the authors studied the thermalization of $N = 4$ SYM plasmas holographically and found analytical black brane solutions to (3.1) with an exponential potential for the scalar fields, as we have explained in previous sections.

The general analytical solution to (3.1) found in [44] at leading order in $1/\tau$ and in the IR limit expressed in our conventions is

$$ds^2 \simeq v^{\frac{2}{6\gamma^2-1}} \left\{ \frac{\tau^{-4\gamma^2}}{1-v^\xi} dv^2 + \tau^{-\frac{2}{3}} \left[-(1-v^\xi) d\tau^2 + \tau^2 dy^2 + dx_\perp^2 \right] \right\} \quad (6.2)$$

and the solution for the scalar field reads

$$e^\phi = \tau \sqrt{\frac{3}{2}} \gamma v^{\frac{3\sqrt{\frac{3}{2}}\gamma}{1-6\gamma^2}}$$

where we defined the scaling variable v as

$$v = \frac{z}{\tau^{\frac{1}{3}-2\gamma^2}}$$

and z is the holographic coordinate. Moreover, we work in the gauge where:

$$\xi = \frac{3}{1-6\gamma^2} + 1. \quad (6.3)$$

In fact, the metric (6.2) is nothing but a black hole solution with moving horizon. This is clearer when we express the metric as a function of z using (6.1) at leading order in $1/\tau$:

$$ds^2 \simeq z^{\frac{2}{6\gamma^2-1}} \left\{ \frac{dz^2}{1-\tau^2\gamma^2-\frac{4}{3}z^\xi} - \left(1 - \tau^2\gamma^2 - \frac{4}{3}z^\xi \right) d\tau^2 + \tau^2 dy^2 + dx_\perp^2 \right\} \quad (6.4)$$

and the scalar field reads:

$$e^\phi = z^{\frac{3\sqrt{\frac{3}{2}}\gamma}{1-6\gamma^2}}.$$

From (6.4) we are able to compute the late time curvatures at the horizon as a function of our parameter γ . In particular, we calculate the Ricci scalar, the squared Ricci tensor and the squared Riemann tensor (i.e. Kretschmann) at leading order in $1/\tau$ evaluated at the horizon:

$$\begin{aligned} R &\simeq \frac{10(3\gamma^2-2)\tau^{4\gamma^2}}{(1-6\gamma^2)^2} \sim \tau^{4\gamma^2} \\ R^2 = R_{\mu\nu}R^{\mu\nu} &\simeq \frac{20(2-3\gamma^2)^2\tau^{8\gamma^2}}{(1-6\gamma^2)^4} \sim \tau^{8\gamma^2} \\ K = R^{\mu\nu\rho\sigma}R_{\mu\nu\rho\sigma} &\simeq \frac{28(2-3\gamma^2)^2\tau^{8\gamma^2}}{(1-6\gamma^2)^4} \sim \tau^{8\gamma^2}. \end{aligned} \quad (6.5)$$

Interestingly, we see from (6.5) that the curvatures at the horizon grow with proper time for several choices of γ at late times, indicating the presence of a curvature singularity at the horizon in the limit where $\tau \rightarrow \infty$. Moreover, the curvatures are singular at $\gamma_c = 1/\sqrt{6}$ and whereas the Kretschmann and squared Ricci tensor keep the same sign, the Ricci scalar changes its sign at precisely $\gamma_M = \sqrt{2/3}$ which is the γ where the potential starts to have a minimum. Unfortunately, the prefactors in front of the curvatures need some correction since they depend on the whole background and our background is different than the one used in [44] in the UV. Nevertheless, we expect the exponents of τ to be correct since in the IR we have the same effective exponential potential as in their action and we expect the black brane solution (6.2) to be a solution of our theory in the late time regime as well.

6.2 Numerical results

In Figure 6.1 we show the numerical results for the simulated curvature invariants evaluated at the horizon. As we can see, the curvature invariants grow with proper time. This observed growth has a straightforward explanation. As the system cools down, the scalar value at the horizon rises, continuing to move down its unbounded potential.

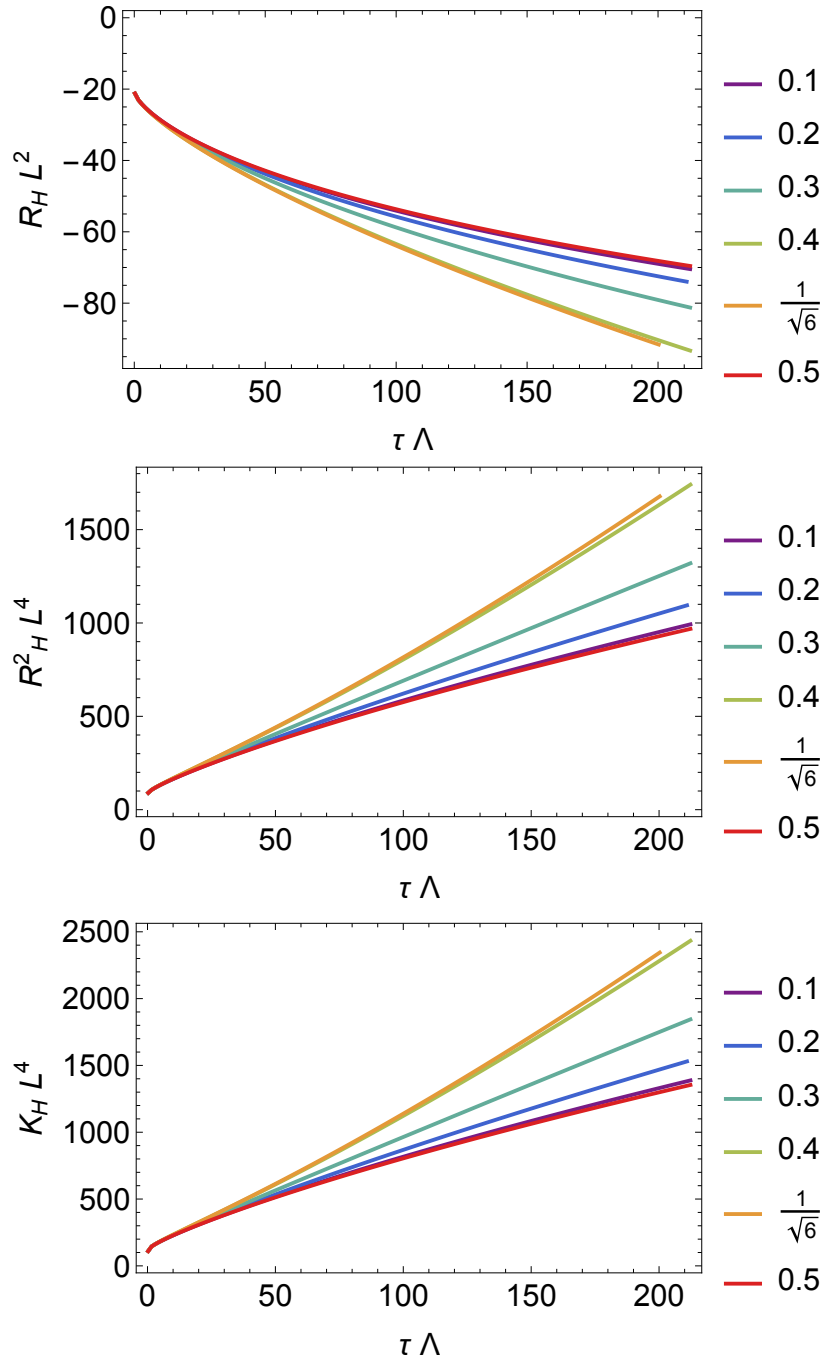


FIGURE 6.1: Ricci scalar, squared Ricci tensor and Kretschmann at the horizon as a function of proper time τ for different choice of γ 's.

As we explained in the previous sections, according to Einstein's equations, the Ricci

scalar at the horizon is proportional to the potential value there, $R_H \propto V(\phi_H)$, suggesting that it will keep increasing. Moreover, as predicted in (6.5) where we took the late time solution found by [44], the curvatures grow arbitrarily at late times when the deep IR regime is reached. In fact, we expect the curvature invariants at the horizon to evolve as

$$R_H \propto \tau^{4\gamma^2}, \quad R_{\mu\nu}R^{\mu\nu}|_H \sim K_H \propto \tau^{8\gamma^2}. \quad (6.6)$$

Here, $K = R_{\mu\nu\rho\sigma}R^{\mu\nu\rho\sigma}$ is the Kretschmann scalar, with the subscript "H" indicating evaluation at the horizon. In the late time limit, we have checked that we recover the predicted behaviors for the curvature invariants evaluated at the horizon.

6.2.1 General vs fined tuned conditions

Lastly, we should consider the generality of our findings. We have shown that a broad range of γ values yield similar physics. Remarkably, our results do not depend on finely tuned initial conditions. This can be seen in Figure 6.2, where even varying the boundary conditions still leads to an evolution well described by first-order hydrodynamics, resulting in the growth of curvatures. In particular, we have chosen different initial conditions while fixing the total energy density for $\gamma = 0.4$.

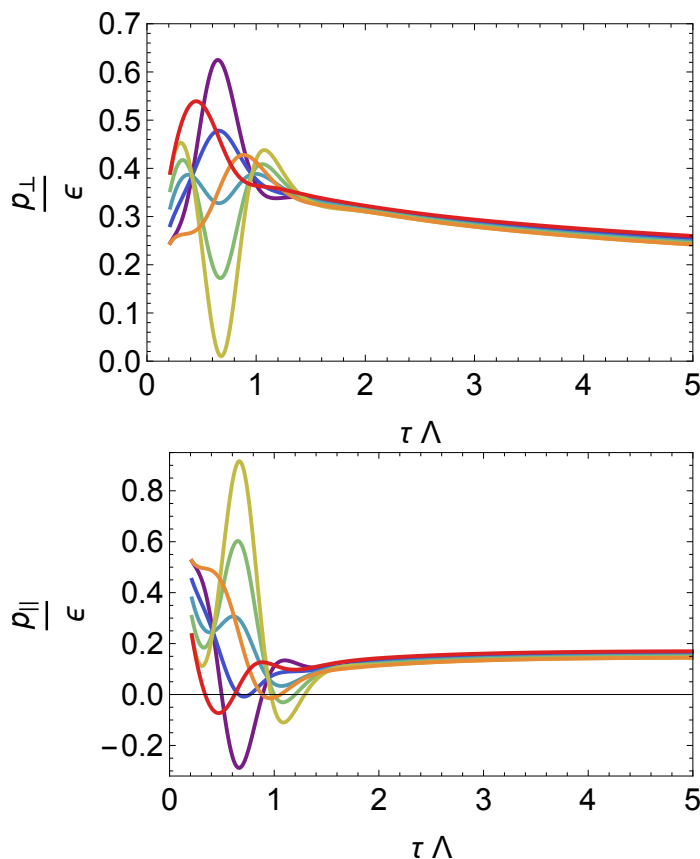


FIGURE 6.2: Initial evolution of the longitudinal and transverse pressures with different initial conditions. We fixed the initial energy and trace of the energy-momentum tensor to be the same.

One might argue that our results may not hold beyond the boost-invariant case. For instance, an unstable quasi-normal mode with finite momentum could challenge our conclusions. We are currently investigating this. However, this is unlikely since

similar models (characterized by exponential growth at low energies) show such instability only at finite chemical potential [24, 23, 9].

Chapter 7

Conclusions and future directions

7.1 Conclusions

Finally, let us discuss what we have done in this Master's thesis:

- We have presented a mechanism which generates arbitrarily high curvatures in boost invariant setups and in asymptotically AdS spacetimes.
- This finding demonstrates that the late-time curvature growth identified in [44] can indeed be realized in UV-complete scenarios without requiring fine-tuned initial conditions.
- Our results highlight a situation where curvature corrections to classical gravity become significant.
- Holography provides a method to investigate these corrections. If such corrections had been incorporated into our action (3.1), the late-time viscosities would differ from those we derived by finite N and finite coupling corrections, as shown in [17].

7.2 Future directions

Our work raises several unresolved questions and opens up numerous potential research directions. Here we mention some of them.

- To provide a more robust argument regarding the stability of black branes, we should study the quasi-normal modes. This involves introducing a metric perturbation and checking if all the quasi-normal modes have negative imaginary frequencies, ensuring the solution's stability.
- Investigate the behaviour for $\gamma > \gamma_c$ to explore the potential phase transitions and GL type instability. For that purpose, we should probably relax some assumptions and symmetries of our ansatz in order for the different phases to be able to exist.
- It would be interesting to extend the work by finding similar solutions in other string theory compactifications.

Bibliography

- [1] Gerard 't Hooft. “A Planar Diagram Theory for Strong Interactions”. In: *Nucl. Phys. B* 72 (1974). Ed. by J. C. Taylor, p. 461. DOI: 10 . 1016 / 0550 - 3213(74) 90154-0.
- [2] Ofer Aharony et al. “Large N field theories, string theory and gravity”. In: *Phys. Rept.* 323 (2000), pp. 183–386. DOI: 10 . 1016 / S0370 - 1573(99) 00083 - 6. arXiv: hep-th/9905111.
- [3] Tomas Andrade, Pau Figueras, and Ulrich Sperhake. “Evidence for violations of Weak Cosmic Censorship in black hole collisions in higher dimensions”. In: *JHEP* 03 (2022), p. 111. DOI: 10 . 1007 / JHEP03(2022) 111. arXiv: 2011 . 03049 [hep-th].
- [4] Tomas Andrade et al. “Entropy production and entropic attractors in black hole fusion and fission”. In: *JHEP* 08 (2020), p. 098. DOI: 10 . 1007 / JHEP08(2020) 098. arXiv: 2005 . 14498 [hep-th].
- [5] Tomás Andrade et al. “Black hole collisions, instabilities, and cosmic censorship violation at large D ”. In: *JHEP* 09 (2019), p. 099. DOI: 10 . 1007 / JHEP09(2019) 099. arXiv: 1908 . 03424 [hep-th].
- [6] Maximilian Attems et al. “Paths to equilibrium in non-conformal collisions”. In: *Journal of High Energy Physics* 2017.6 (June 2017). ISSN: 1029-8479. DOI: 10 . 1007 / jhep06(2017) 154. URL: [http://dx.doi.org/10.1007/JHEP06\(2017\)154](http://dx.doi.org/10.1007/JHEP06(2017)154).
- [7] Jacob D. Bekenstein. “Black holes and entropy”. In: *Phys. Rev. D* 7 (1973), pp. 2333–2346. DOI: 10 . 1103/PhysRevD.7.2333.
- [8] Iosif Bena et al. “Holographic dual of hot Polchinski-Strassler quark-gluon plasma”. In: *JHEP* 09 (2019), p. 033. DOI: 10 . 1007 / JHEP09(2019) 033. arXiv: 1805 . 06463 [hep-th].
- [9] Panagiotis Betzios et al. “Quasinormal modes of a strongly coupled nonconformal plasma and approach to criticality”. In: *Phys. Rev. D* 97.8 (2018), p. 081901. DOI: 10 . 1103/PhysRevD.97.081901. arXiv: 1708 . 02252 [hep-th].
- [10] Massimo Bianchi, Daniel Z. Freedman, and Kostas Skenderis. “Holographic renormalization”. In: *Nucl. Phys. B* 631 (2002), pp. 159–194. DOI: 10 . 1016 / S0550-3213(02)00179-7. arXiv: hep-th/0112119.
- [11] Massimo Bianchi, Daniel Z. Freedman, and Kostas Skenderis. “How to go with an RG flow”. In: *JHEP* 08 (2001), p. 041. DOI: 10 . 1088/1126-6708/2001/08/041. arXiv: hep-th/0105276.
- [12] J. D. Bjorken. “Highly Relativistic Nucleus-Nucleus Collisions: The Central Rapidity Region”. In: *Phys. Rev. D* 27 (1983), pp. 140–151. DOI: 10 . 1103 / PhysRevD.27.140.
- [13] H. Bondi. “Gravitational Waves in General Relativity”. In: *Nature* 186.4724 (1960), pp. 535–535. DOI: 10 . 1038/186535a0.

- [14] H. Bondi, M. G. J. van der Burg, and A. W. K. Metzner. "Gravitational waves in general relativity. 7. Waves from axisymmetric isolated systems". In: *Proc. Roy. Soc. Lond. A* 269 (1962), pp. 21–52. DOI: 10.1098/rspa.1962.0161.
- [15] John P Boyd. *Chebyshev and Fourier spectral methods*. Courier Corporation, 2001.
- [16] Peter Breitenlohner and Daniel Z. Freedman. "Positive Energy in anti-De Sitter Backgrounds and Gauged Extended Supergravity". In: *Phys. Lett. B* 115 (1982), pp. 197–201. DOI: 10.1016/0370-2693(82)90643-8.
- [17] Alex Buchel. "Holographic Gauss-Bonnet transport". In: *Phys. Lett. B* 853 (2024), p. 138666. DOI: 10.1016/j.physletb.2024.138666. arXiv: 2402.16109 [hep-th].
- [18] Jorge Casalderrey-Solana et al. "Hawking temperature of a general black brane metric". In: *Gauge/String Duality, Hot QCD and Heavy Ion Collisions*. Cambridge University Press, 2014, pp. 405–405.
- [19] Jorge Casalderrey-Solana et al. "Strong-coupling dynamics and entanglement in de Sitter space". In: *JHEP* 03 (2021), p. 181. DOI: 10.1007/JHEP03(2021)181. arXiv: 2011.08194 [hep-th].
- [20] Paul M. Chesler and Laurence G. Yaffe. "Holography and colliding gravitational shock waves in asymptotically AdS₅ spacetime". In: *Phys. Rev. Lett.* 106 (2011), p. 021601. DOI: 10.1103/PhysRevLett.106.021601. arXiv: 1011.3562 [hep-th].
- [21] Paul M. Chesler and Laurence G. Yaffe. "Horizon Formation and Far-from-Equilibrium Isotropization in a Supersymmetric Yang-Mills Plasma". In: *Physical Review Letters* 102.21 (May 2009). ISSN: 1079-7114. DOI: 10.1103/physrevlett.102.211601. URL: <http://dx.doi.org/10.1103/PhysRevLett.102.211601>.
- [22] Paul M. Chesler and Laurence G. Yaffe. "Numerical solution of gravitational dynamics in asymptotically anti-de Sitter spacetimes". In: *Journal of High Energy Physics* 2014.7 (July 2014). ISSN: 1029-8479. DOI: 10.1007/jhep07(2014)086. URL: [http://dx.doi.org/10.1007/JHEP07\(2014\)086](http://dx.doi.org/10.1007/JHEP07(2014)086).
- [23] Jesús Cruz Rojas, Tuna Demircik, and Matti Järvinen. "Modulated instabilities and the AdS₂ point in dense holographic matter". In: (May 2024). arXiv: 2405.02399 [hep-th].
- [24] Tuna Demircik et al. "Is holographic quark-gluon plasma homogeneous?" In: (May 2024). arXiv: 2405.02392 [hep-ph].
- [25] M. J. Duff and James T. Liu. "Anti-de Sitter black holes in gauged N = 8 supergravity". In: *Nucl. Phys. B* 554 (1999), pp. 237–253. DOI: 10.1016/S0550-3213(99)00299-0. arXiv: hep-th/9901149.
- [26] Daniel Elander et al. "Phase transitions in a three-dimensional analogue of Klebanov-Strassler". In: *JHEP* 06 (2020), p. 131. DOI: 10.1007/JHEP06(2020)131. arXiv: 2002.08279 [hep-th].
- [27] Christopher Eling and Yaron Oz. "A Novel Formula for Bulk Viscosity from the Null Horizon Focusing Equation". In: *JHEP* 06 (2011), p. 007. DOI: 10.1007/JHEP06(2011)007. arXiv: 1103.1657 [hep-th].
- [28] Antón F. Faedo et al. "Light holographic dilatons near critical points". In: (June 2024). arXiv: 2406.04974 [hep-th].

- [29] Pau Figueras et al. “Endpoint of the Gregory-Laflamme instability of black strings revisited”. In: *Physical Review D* 107.4 (Feb. 2023). ISSN: 2470-0029. DOI: 10.1103/PhysRevD.107.044028. URL: <http://dx.doi.org/10.1103/PhysRevD.107.044028>.
- [30] D. Z. Freedman et al. “Continuous distributions of D3-branes and gauged supergravity”. In: *JHEP* 07 (2000), p. 038. DOI: 10.1088/1126-6708/2000/07/038. arXiv: hep-th/9906194.
- [31] D. Z. Freedman et al. “Renormalization group flows from holography supersymmetry and a c theorem”. In: *Adv. Theor. Math. Phys.* 3 (1999), pp. 363–417. DOI: 10.4310/ATMP.1999.v3.n2.a7. arXiv: hep-th/9904017.
- [32] François Gelis. “Some aspects of the theory of heavy ion collisions”. In: *Reports on Progress in Physics* 84.5 (Apr. 2021), p. 056301. ISSN: 1361-6633. DOI: 10.1088/1361-6633/abec2e. URL: <http://dx.doi.org/10.1088/1361-6633/abec2e>.
- [33] G. W. Gibbons and S. W. Hawking. “Action Integrals and Partition Functions in Quantum Gravity”. In: *Phys. Rev. D* 15 (1977), pp. 2752–2756. DOI: 10.1103/PhysRevD.15.2752.
- [34] L. Girardello et al. “Novel local CFT and exact results on perturbations of N=4 superYang Mills from AdS dynamics”. In: *JHEP* 12 (1998), p. 022. DOI: 10.1088/1126-6708/1998/12/022. arXiv: hep-th/9810126.
- [35] Michael B. Green, J. H. Schwarz, and Edward Witten. *SUPERSTRING THEORY. VOL. 1: INTRODUCTION*. Cambridge Monographs on Mathematical Physics. July 1988. ISBN: 978-0-521-35752-4.
- [36] R. Gregory and R. Laflamme. “Black strings and p-branes are unstable”. In: *Phys. Rev. Lett.* 70 (1993), pp. 2837–2840. DOI: 10.1103/PhysRevLett.70.2837. arXiv: hep-th/9301052.
- [37] Ruth Gregory and Raymond Laflamme. “The Instability of charged black strings and p-branes”. In: *Nucl. Phys. B* 428 (1994), pp. 399–434. DOI: 10.1016/0550-3213(94)90206-2. arXiv: hep-th/9404071.
- [38] S. S. Gubser, Igor R. Klebanov, and Alexander M. Polyakov. “Gauge theory correlators from noncritical string theory”. In: *Phys. Lett. B* 428 (1998), pp. 105–114. DOI: 10.1016/S0370-2693(98)00377-3. arXiv: hep-th/9802109.
- [39] Steven S. Gubser. “Curvature singularities: The Good, the bad, and the naked”. In: *Adv. Theor. Math. Phys.* 4 (2000), pp. 679–745. DOI: 10.4310/ATMP.2000.v4.n3.a6. arXiv: hep-th/0002160.
- [40] Steven S. Gubser and Abhinav Nellore. “Mimicking the QCD equation of state with a dual black hole”. In: *Phys. Rev. D* 78 (2008), p. 086007. DOI: 10.1103/PhysRevD.78.086007. arXiv: 0804.0434 [hep-th].
- [41] U. Gursoy and E. Kiritsis. “Exploring improved holographic theories for QCD: Part I”. In: *JHEP* 02 (2008), p. 032. DOI: 10.1088/1126-6708/2008/02/032. arXiv: 0707.1324 [hep-th].
- [42] U. Gursoy, E. Kiritsis, and F. Nitti. “Exploring improved holographic theories for QCD: Part II”. In: *JHEP* 02 (2008), p. 019. DOI: 10.1088/1126-6708/2008/02/019. arXiv: 0707.1349 [hep-th].
- [43] Umut Gursoy. “Continuous Hawking-Page transitions in Einstein-scalar gravity”. In: *JHEP* 01 (2011), p. 086. DOI: 10.1007/JHEP01(2011)086. arXiv: 1007.0500 [hep-th].

- [44] Umut Gursoy, Matti Jarvinen, and Giuseppe Policastro. “Late time behavior of non-conformal plasmas”. In: *JHEP* 01 (2016), p. 134. DOI: 10 . 1007 / JHEP01(2016)134. arXiv: 1507 . 08628 [hep-th].
- [45] Sebastian de Haro, Sergey N. Solodukhin, and Kostas Skenderis. “Holographic reconstruction of space-time and renormalization in the AdS / CFT correspondence”. In: *Commun. Math. Phys.* 217 (2001), pp. 595–622. DOI: 10 . 1007 / s002200100381. arXiv: hep-th/0002230.
- [46] M. Henningson and K. Skenderis. “The Holographic Weyl anomaly”. In: *JHEP* 07 (1998), p. 023. DOI: 10 . 1088 / 1126 - 6708 / 1998 / 07 / 023. arXiv: hep-th / 9806087.
- [47] Edmond Iancu. *QCD in heavy ion collisions*. 2012. arXiv: 1205 . 0579 [hep-ph].
- [48] Romuald A. Janik and Robi Peschanski. “Asymptotic perfect fluid dynamics as a consequence of AdS/CFT correspondence”. In: *Physical Review D* 73.4 (Feb. 2006). ISSN: 1550-2368. DOI: 10 . 1103 / physrevd . 73 . 045013. URL: <http://dx.doi.org/10.1103/PhysRevD.73.045013>.
- [49] Matti Jarvinen and Elias Kiritsis. “Holographic Models for QCD in the Veneziano Limit”. In: *JHEP* 03 (2012), p. 002. DOI: 10 . 1007 / JHEP03(2012)002. arXiv: 1112 . 1261 [hep-ph].
- [50] Barak Kol. “Topology change in general relativity, and the black hole black string transition”. In: *JHEP* 10 (2005), p. 049. DOI: 10 . 1088 / 1126 - 6708 / 2005 / 10 / 049. arXiv: hep-th/0206220.
- [51] Juan Martin Maldacena. “The Large N limit of superconformal field theories and supergravity”. In: *Adv. Theor. Math. Phys.* 2 (1998), pp. 231–252. DOI: 10 . 4310 / ATMP . 1998 . v2 . n2 . a1. arXiv: hep-th/9711200.
- [52] R. Penrose. “Gravitational collapse: The role of general relativity”. In: *Riv. Nuovo Cim.* 1 (1969), pp. 252–276. DOI: 10 . 1023 / A : 1016578408204.
- [53] J. Polchinski. *String theory. Vol. 1: An introduction to the bosonic string*. Cambridge Monographs on Mathematical Physics. Cambridge University Press, Dec. 2007. ISBN: 978-0-511-25227-3, 978-0-521-67227-6, 978-0-521-63303-1. DOI: 10 . 1017 / CB09780511816079.
- [54] G. Policastro, Dan T. Son, and Andrei O. Starinets. “The Shear viscosity of strongly coupled N=4 supersymmetric Yang-Mills plasma”. In: *Phys. Rev. Lett.* 87 (2001), p. 081601. DOI: 10 . 1103 / PhysRevLett . 87 . 081601. arXiv: hep-th/0104066.
- [55] Frans Pretorius. “Evolution of Binary Black-Hole Spacetimes”. In: *Physical Review Letters* 95.12 (Sept. 2005). ISSN: 1079-7114. DOI: 10 . 1103 / physrevlett . 95 . 121101. URL: <http://dx.doi.org/10.1103/PhysRevLett.95.121101>.
- [56] R. K. Sachs. “Gravitational waves in general relativity. 8. Waves in asymptotically flat space-times”. In: *Proc. Roy. Soc. Lond. A* 270 (1962), pp. 103–126. DOI: 10 . 1098 / rspa . 1962 . 0206.
- [57] Wilke van der Schee. “Gravitational collisions and the quark-gluon plasma”. PhD thesis. Utrecht U., 2014. arXiv: 1407 . 1849 [hep-th].
- [58] Wilke van der Schee. “Holographic thermalization with radial flow”. In: *Phys. Rev. D* 87.6 (2013), p. 061901. DOI: 10 . 1103 / PhysRevD . 87 . 061901. arXiv: 1211 . 2218 [hep-th].

- [59] Evgeny Sorkin. "A Critical dimension in the black string phase transition". In: *Phys. Rev. Lett.* 93 (2004), p. 031601. DOI: 10.1103/PhysRevLett.93.031601. arXiv: hep-th/0402216.
- [60] Robert M. Wald. "Gravitational collapse and cosmic censorship". In: Oct. 1997, pp. 69–85. DOI: 10.1007/978-94-017-0934-7_5. arXiv: gr-qc/9710068.
- [61] Edward Witten. "Anti-de Sitter space and holography". In: *Adv. Theor. Math. Phys.* 2 (1998), pp. 253–291. DOI: 10.4310/ATMP.1998.v2.n2.a2. arXiv: hep-th/9802150.
- [62] Edward Witten. "Baryons in the $1/n$ Expansion". In: *Nucl. Phys. B* 160 (1979), pp. 57–115. DOI: 10.1016/0550-3213(79)90232-3.
- [63] Edward Witten. "Reflections on the fate of space-time". In: *Phys. Today* 49N4 (1996). Ed. by C. Callender and N. Huggett, pp. 24–30. DOI: 10.1063/1.881493.